UNIVERSITY OF CALIFORNIA

Radiation Laboratory

BERKELEY, CALIFORNIA

DISCLAIMER

UCRL-3449

UNIVERSITY OF CALIFORNIA
Radiation Laboratory
Berkeley, California

Contract No. W-7405-eng-48

π^0 MODES OF HEAVY-MESON AND HYPERON DECAY

John E. Osher

(Thesis)

June 22, 1956

Printed for the U. S. Atomic Energy Commission

π^0 MODES OF HEAVY-MESON AND HYPERON DECAY

Contents

π^0 MODES OF HEAVY-MESON AND HYPERON DECAY

John E. Osher

Radiation Laboratory
University of California
Berkeley, California

June 22, 1956

ABSTRACT

π^0 modes of heavy-meson and hyperon decay have been investigated at the Berkeley Bevatron. The Bevatron proton beam was allowed to produce heavy mesons and hyperons in a thin copper target; a well-collimated counter telescope was used to observe high-energy gamma rays, originating in defined regions of space near the target, that result from π^0 modes of decay of the heavy mesons and hyperons. The projected spacewise gamma-counting rate was determined by moving the counter telescope and collimation (maintained at 90° lab) on a track parallel to the beam direction. The resulting data were then compared to those predicted by applying the kinematics involved for various assumed models consistent with associated production.

The counting rate found upstream and downstream from the target is consistent with the identification of $\theta^0 \rightarrow \pi^0 + \pi^0$, which requires the θ^0 to have even spin and parity. The analysis of the data gave a mean lifetime of $1.9^{+.2}_{-.3} \times 10^{-10}$ sec, an angular-distribution best fit for $\cos^{14}\theta_{c.m.}$, and an energy dependence approximately proportional to $\left\{\left(\frac{E_\theta}{M_\theta}\right)^2 - 1\right\}_{c.m.}$. The above matrix-element dependences yield a cross section of $0.22 \pm .07$ mb per nucleon in copper averaged for 5.7- to 6.2-Bev protons, and this implies a decay branching ratio of order unity. The experimental data also indicate a contribution for some mixture of $\theta^+ \rightarrow \pi^+ + \pi^0$, $\Sigma^+ \rightarrow p + \pi^0$, and $\Lambda^0 \rightarrow n + \pi^0$.

π^0 MODES OF HEAVY-MESON AND HYPERON DECAY

John E. Osher

Radiation Laboratory
University of California
Berkeley, California

June 22, 1956

I. INTRODUCTION

A. Statement of the Problem

In recent years the investigation of the mechanics of production, interaction, and decay of heavy mesons and hyperons has become an active field of research. This research (summarized below in section I-B) has in general allowed one class of decay for neutral heavy mesons and hyperons to go undetermined; that is, for some of these new particles there is the possibility of neutral decay modes, competing with the charged modes ordinarily observed, which had gone unobserved owing to extremely poor detection efficiency in normal cloud-chamber and emulsion experiments. It is the purpose of this counter experiment to identify those particles having such alternate decay modes, which include at least one π^0 meson and hence yield high-energy gamma rays. Such an identification allows an analysis of the data for the decay branching ratios, the lifetime, and production mechanism for the particle identified.

B. Background

The investigation of the properties of heavy mesons and hyperons started in 1947 when the first clear evidence for new "curious" particles was found by Rochester and Butler.[1] In the early cosmic-ray experiments the interesting events fell into two classes: the "V events" (the appearance of a V-shaped track) denoting decays in flight, and the "S events" denoting the stopping of charged particles with subsequent decay. Each of these types of events was later found to be a mixture of

two distinct groups of particles: a group labeled heavy mesons (general notation K, with individual varieties given small Greek letters) and a group labeled hyperons (general notation Y, with individual varieties given capital Greek letters). By definition a heavy meson has a mass between that of a meson and a nucleon, and a hyperon has a mass heavier than a nucleon. Within these groups a combination of emulsion, cloud-chamber, and recent counter work[2, 3] has established the common decay characteristics--such as lifetime, decay products, and energy release "Q"--for a number of specific varieties of the new particles. A summary of this work up to May 1956 is given in the table below. It should be noted that several of the new particles were also presumed to have neutral decay modes (e.g., $\theta^0 \rightarrow \pi^0 + \pi^0$ and $\Lambda^0 \rightarrow n + \pi^0$), but they are not included in the table because they had not been experimentally verified at the time it was compiled.

Particle	Symbol	Mass (Mev)	Mean Lifetime (Sec.)	Mode of Decay	Q (Mev)
Heavy	$\tau^{\pm}$	966.3±.5	$1.3^{+.2}_{-.2}\times10^{-8}$	$\tau^{\pm}\rightarrow\pi^{\pm}+\pi^{+}+\pi^{-}$	75.1±.2
Mesons	τ'	961±10	$\sim1.3\times10^{-8}$	$\tau'^{\pm}\rightarrow\pi^{\pm}+\pi^{0}+\pi^{0}$	~75
	θ^0	965±5	$1.7^{+.7}_{-.4}\times10^{-10}$ [a]	$\theta^0\rightarrow\pi^{+}+\pi^{-}$	214±3
	$K^{+}_{\pi_2}$ (θ^{+})	966±1.5	$1.2\pm.1\times10^{-8}$	$K^{+}_{\pi_2}\rightarrow\pi^{+}+\pi^{0}$	219±4
	$K^{-}_{\pi_2}$	963±12	$.95\pm.4\times10^{-8}$	$K^{-}_{\pi_2}\rightarrow\pi^{-}+\pi^{0}$	
	K_{μ_2}	965±2	$1.2\pm.8\times10^{-8}$	$K_{\mu_2}\rightarrow\mu^{+}+\nu$	390±3.5
	K_{μ_3}	966±6	$\sim10^{-8}$	$K_{\mu_3}\rightarrow\mu^{+}+?+?$	
	K_{e_3}	961±10	$\sim10^{-8}$	$K_{e_3}\rightarrow e^{+}+?+?$	
Hyperons	Ξ^{-}	2585±6	$\sim10^{-10}$	$\Xi^{-}\rightarrow\Lambda^{0}+\pi^{-}$	66.5±3
	Σ^{+}	2327±1	$.34^{+.2}_{-.1}\times10^{-10}$	$\Sigma^{+}\rightarrow n+\pi^{+}\ (p+\pi^{0})$	116±.5
	Σ^{-}	2338±6	$1.4^{+.6}_{-.3}\times10^{-10}$	$\Sigma^{-}\rightarrow n+\pi^{-}$	118+3
	Σ^{0} (?)	2340±60	$<10^{-11}$	$\Sigma^{0}\rightarrow\Lambda^{0}+\gamma$	80±30
	Λ^0	2182±.4	$3.7\pm6\times10^{-10}$	$\Lambda^0\rightarrow p+\pi^{-}$	37±.2

[a] See Section V-C

In addition to the common decay properties, other characteristics such as production and interaction were available from the data. The production threshold experiments indicated clearly that production started only at energies considerably greater than that necessary for a single K meson or Y hyperon. In fact, the threshold appeared to occur at such an energy that a K + Y could be simultaneously produced, and the specific production events that have been seen support this "associated" production (there is also evidence for some K + Y + π production[4]). The cross section for "associated" production appears to be near 1 mb at high energies, which requires a coupling of the same order of magnitude as π mesons for these new particles. The strong coupling has also been borne out by K-meson scattering in emulsions (K^- approximately geometric cross section and K^+ approximately 1/3 geometric cross section)[5] and by extensive hyperfragment data for Λ^0 hyperons bound to various nuclei with binding energies comparable to an equivalent bound neutron.

It should be noted that the experimental data present several profound theoretical problems. First of all, simple theoretical calculations for ordinary gamma or pion decay modes of heavy mesons or hyperons yield lifetimes of from 10^{-18} to 10^{-21} second instead of the observed 10^{-8} to 10^{-12} second. Secondly, apparent need for associated production presents a problem compounded by the absence of associated Y + Y production (or K + K). Finally, the apparent number of heavy mesons and hyperons adds a complication (which may be somewhat simplified, however, when the mysterious degeneracy that exists among the heavy-meson masses and some of their lifetimes is resolved). The degeneracy in lifetime (e.g., in K_{π_2}, τ, and K_{μ_2}) certainly suggests that a single fundamental particle is responsible for several decay schemes.

This then summarizes the information to be reduced by some fundamental theory. To this end Gell-Mann's theory of "strangeness"[6] gives a simple fit to experimental results, though several other theories[7, 8, 9] on this subject do exist and lead in general through

different justifications to identical conclusions. Gell-Mann's theory of "strangeness" starts with a framework of three basic forms of interaction:

1. The "strong" interactions, which are responsible for nuclear forces or production of π mesons and K mesons in high-energy collisions. This form of interaction is confined to baryons (nucleons and all known hyperons), antibaryons, π mesons, and heavy mesons. This type of interaction involves charge independence, conserving total isotopic spin I, and the Z component of isotopic spin I_Z.

2. The electromagnetic interactions linking photons to charges and currents. This type of interaction is responsible for photopion production and in general conserves I_Z but not I.

3. The weak interactions responsible for β decay, the slow decay of heavy mesons and hyperons, and the meson decay.

In addition Gell-Mann generalizes the concept of charge independence to the extent that values of isotopic spin are assigned to the various heavy mesons and hyperons; however, the charge multiplets have displaced charge centers. That is, the new relation between the charge and isotopic spin for a particle or system of particles is $Q/e = I_Z + N/2 + S/2$, where N is the number of baryons minus the number of antibaryons and S is a new quantum number called "strangeness" (the value of S is of course directly responsible for charge displacement of charge multiplets). Under this formalism strong interactions conserve I, I_Z, N, and S; electro-magnetic interactions conserve I_Z, N, and S; and weak interactions allow violation of conservation of S, giving a rule of $\Delta S = \pm 1$ for weak interactions. The assignment of values of S to the various elementary particles follows on the next page. Note that the ordinary particles have $S = 0$, while the new or "strange" particles have values of $S \neq 0$, hence the name strangeness.

Particle Multiplet	Mass (M_π)	S	I
K^+, K^0	3.54	+1	1/2
$n, \bar{n}$	6.7	0	1/2
π	1	0	1
$K^-, \bar{K}^0$	3.54	-1	1/2
Λ^0	8.0	-1	0
$\Sigma^{\pm, 0}$	8.55	-1	1
$\Xi^-, 0$	9.5	-2	1/2

With these assignments of strangeness and the rule for conservation of S except in weak interactions, the theoretical postulate may be summarized by the following laws.

1. The law of stability requires that a strange particle cannot decay into ordinary (S = 0) particles except through the slow weak interaction.

2. The law of associated production states that two or more strange particles may be produced in a collision of ordinary particles, and that the net sum of S must equal zero in the reaction for rapid production; hence, single production of strange particles is forbidden.

In addition, the theory postulates the existence of Ξ^0, Σ^0 hyperons to complete multiplet systems, though these predicted hyperons have fast allowed electromagnetic transitions that make experimental verification difficult. Also a degeneracy in K mesons arises from the apparent best fit of a τ meson to zero spin and odd parity, while the θ family has even spin and even parity (probably zero spin and even parity). As a result the doublet systems of K^+ and K^0 and of K^- and $\bar{K}^0$ are presumably paralleled by τ^+ and τ^0 and by τ^- and $\bar{\tau}^0$.

The position of the heavy mesons and hyperons in modern nuclear physics becomes important for the high-energy reactions. This results simply from the large energy needed for real states of these particles, and this large energy makes the position of the virtual states

insignificant, compared with pion states, for low-energy interactions. For high-energy interactions, on the other hand, the K's and Y's should be responsible for strong short-range forces contributing to nuclear interactions. These contributions depend on the variety, characteristic internal structure, and interactions of these particles. These are indeed the properties under current early experimental investigation. To date the major role of these new "strange" particles has been to develop a broadening of theoretical views in attempts to understand the unusual properties of these particles.

The background material of direct application to this experiment stems from both previous experiment and theory. Experimental data furnish rather explicit expected decay models for the known strange particles. That is, masses and Q value are rather accurately known, lifetimes are roughly known, and π^0 decay modes analogous to observed charged decay modes could be inferred. Also, for an analysis of the spatial decay rate as experimentally determined, it was necessary that the essential features of the kinematics involved be known. One requirement of this was knowledge of the production processes, and the assumption used here was based on "associated production" (inferred from essentially all machine experiments) as given by Gell-Mann's theory of strangeness. This theory allows the following classes of "associated" production in nucleon-nucleon collisions, where care must be taken in the choice of allowed particles such that the strangeness of the total reaction is zero. (It should be noted that the classes listed each contain two or more strange particles, hence the name "associated".) Here the letter K is used to indicate a heavy meson, Λ, Σ, and Ξ to indicate hyperons (general inclusive notation, Y), and n to denote a nucleon.

Class	Threshold for Free Nucleon (Bev)	Threshold for Fermi Momentum Distrib. with -24 Mev Limit (Bev)
$p + n \rightarrow n + \Lambda + K$	1.55	1.15
$p + n \rightarrow n + \Sigma + K$	1.85	1.3
$p + n \rightarrow n + n + K + \bar{K}$	2.8	2.1
$p + n \rightarrow n + \Xi + K + K$	3.65	2.9

On the basis of lower threshold and lower multiplicity (greater phase-space volume), the general form of associated production assumed to predominate was $n + n \rightarrow N + Y + K$. Indirect production through π mesons was taken to be unimportant except near threshold, owing to the two cross sections involved and to the multiplicity of pionproduction, which generally keeps the meson energies below or near threshold for the indirect processes. The crude shape of the excitation function near threshold and the "disappearance" of the K-meson upstream decay contribution near 3 Bev, as observed in this experiment, appear consistent with this assumption.

C. Experimental Method

The technique used in this counter experiment depends upon the production of heavy mesons and hyperons in a localized region (thin target) and on the fact that their lifetimes are such that (with available laboratory kinetic energies and time dilation) these particles commonly decay some centimeters from the target. The counter was collimated to observe decay products resulting from well-localized regions of space. The decay products of particular interest here were π^0 mesons, which decay essentially instantaneously (approximately 2×10^{-15} second) into two high-energy gamma rays; hence, the counter used was a gamma-ray counter telescope. This counter and collimation assembly then were moved along the beam direction upstream and downstream from the target to determine the spatial variation in decay events as projected along the beam direction. These population measurements yield the lifetimes and production characteristics of the particles involved when compared with the predicted variation found on the basis of the expected kinematics and known counter efficiency. In the analysis, the angular distribution for production of the heavy mesons was picked for a best fit to the experimental upstream and downstream contributions.

Considerations for the calculation of the kinematics are outlined in IV-A and given in greater detail in the Appendix.

II. EXPERIMENTAL ARRANGEMENT

A. Physical Layout at Bevatron

The experiment was performed at the Bevatron, with a well-collimated vertical counter array to observe regions near a target bombarded by the internal proton beam. The counter and collimation assembly as a rigid unit (Fig. 1) were mounted on tracks located over a "well" at the west tangent tank of the Bevatron. This location allowed the first collimation aperture to be located within 10 inches of the target, yet the well was of sufficient size to allow movement of the counter and collimation assembly along the tracks parallel to the beam direction over 15 cm either upstream or downstream from the target location. A plan view showing the over-all Bevatron layout and a typical collimotor view is given in Fig. 2.

1. Bevatron Beam and Target

In this experiment, as for most counter experiments, the internal spilled proton beam at the Bevatron was used to decrease the instantaneous counting rates to a point commensurate with the 10^{-8}- to 10^{-9}-sec resolution times of the counter electronics. The beam pulse was spilled over 90 msec instead of the usual 2 msec (or less) by injecting noise into the rf system at the proper time near the end of the acceleration cycle. This time dispersion led to a known energy spread for this experiment of 5.7 to 6.2 Bev, but allowed use of beams of near 10^{10} protons per Bevatron pulse. The proton energy was determined from the magnetic field strength which was monitored by a system of "I" pip markers.

The target and clipper system used at the Bevatron are of the plunging type, since full Bevatron aperture is required up to several hundred Mev and yet the final accelerated beam has shrunk to a cross section of approximately 1 by 4 in. located in a good-field region considerably smaller than full aperture. The solution has been to plunge a target, after the oscillation of the large early beam has died down, to a position near the constricted beam and then shrink or steer the

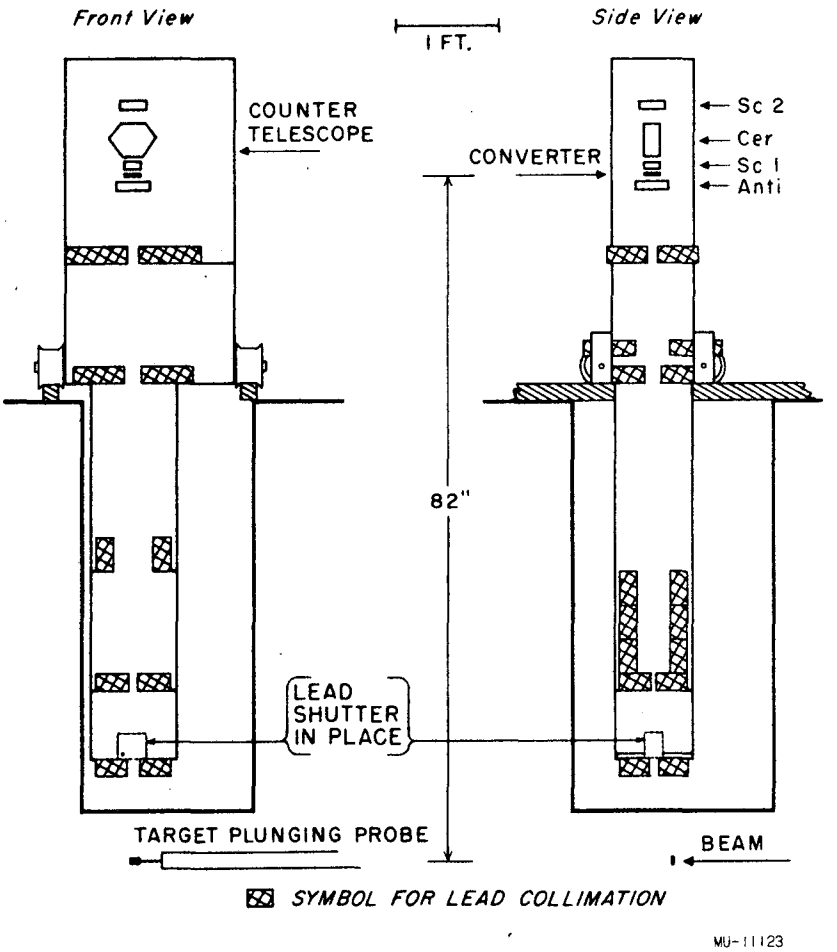

Fig. 1. Counter and collimation assembly.

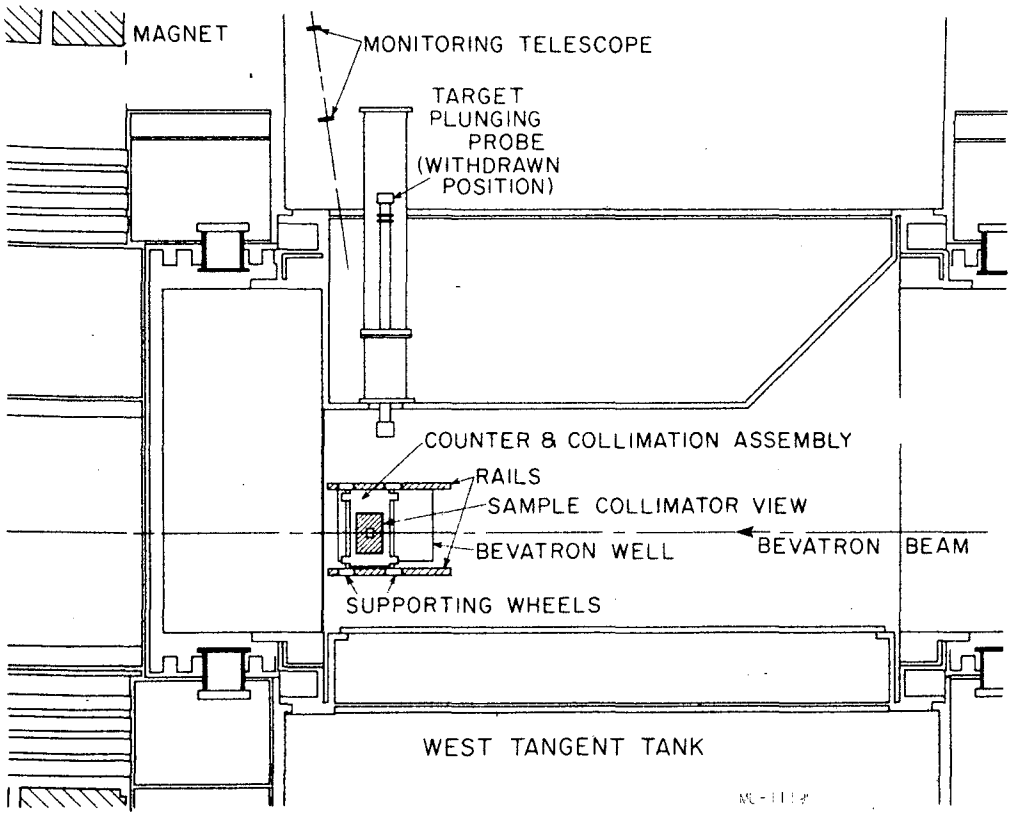

Fig. 2. Experimental layout at Bevatron.

beam into the target. In addition to this complication, a thick copper clipper was similarly plunged 180° from the target (around the machine) to remove the portion of the beam that had been moved radially inward more than a few inches from the target tip. This was important, as the monitoring telescope could see somewhat more of the target than just the final 1/2 in. of the target tip that was in proper geometry for the counter telescope. For example, a target 1/8 in. along beam direction was plunged at the west inside plunging probe position to 599-3/8 in. and the clipper to 597-7/8 in. radius for this experiment, allowing an average of 2.8 proton traversals through the 1/8-in. target before clipping. The beam distribution on this target (under the above conditions) was checked by counting a thin aluminum foil attached to the target (III-C). This indicated that more than 87% of the average 2.8 beam traversals occurred in the first 1/2 in. of the target tip.

B. Counter Telescope

A counter telescope was used as the detector for the high-energy gammas resulting from decay products of heavy mesons and hyperons. The telescope consisted of an array of counters as shown in Fig. 3: respectively, a front plastic scintillator (Anti), a lead converter, a defining plastic scintillator (Sc. 1), a Cerenkov Counter, and a rear plastic scintillator (Sc. 2). The sequence of events for a detected gamma was no pulse from the oversize front counter, conversion of the gamma to an electron and positron pair in the lead converter, and the passage of at least one resulting charged particle through the defining counter, through the Cerenkov counter and into the rear counter. A charged particle with a $\beta > 0.67$ would of course give a pulse in each of the counters, but slower charged particles (e.g., knock-on protons from neutron background) would not trip the Cerenkov counter. This telescope arrangement was the result of previous cooperative work at the cyclotron on another π^0 experiment.[10] The counter telescope components, the associated photomultiplier tubes and magnetic shielding were rigidly mounted as a subunit on an aluminum frame, with the collimation assembly in the location shown in Fig. 1. The converter

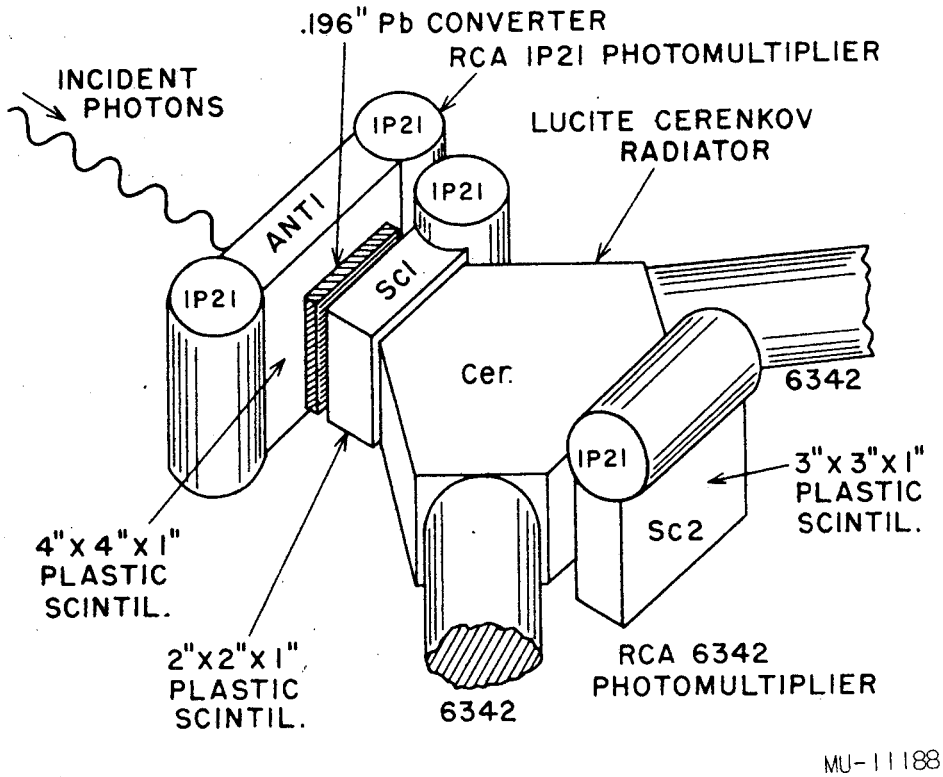

Fig. 3. Gamma-counter telescope.

used in the counter telescope could be moved to standard "in" and "out" positions by a small electric motor and gear arrangement. This allowed a simple correction for neutron events and for gamma conversions other than in the lead converter.

1. Specific Components of the Telescope

a. Scintillation Counter.[11] The plastic scintillator used consisted of a solid solution of terphenyl and tetraphenyl-butadiene frequency shifter in a polystyrene medium. The output is about 40% that of anthracene, with a decay time of 4 millimicroseconds. The defining 2-by-2-by-1-in. counter Sc. 1 and rear 3-by-3-by-1-in. counter Sc. 2 were each viewed by a single 1P21 photomultiplier; the front or "anti" 4-by-4 by 1-in. counter was viewed by two 1P21 photomultipliers. Each of the plastic scintillators had loose aluminum wraps to aid in light collection through a short air gap to the phototube. Connections to the electronics were through 100-foot 125-Ω cables.

b. Cerenkov Counter.[12] The 2-by-2-in.-aperture Cerenkov counter used was designed for consistent pulse output for a reasonably sort path length, chosen here as 10 cm. The geometry was designed so that the Cerenkov cone for a $\beta \tilde{=} 1$ normally incident particle was at nearly normal incidence on the flat photocathodes of the 2-in. photomultiplier tubes used as indicated in Fig. 3. The lucite block was viewed by two RCA 6342 photomultipliers, and in this case mineral oil was injected (through the short rubber sleeve couplings) between the 2-in photomultiplier faces and the 2-in-diameter extensions to the lucite counter block to serve as optical coupling for the light formed in the lucite block. A summary of the theory and use of Cerenkov counters is given in Progress of Nuclear Physics, Volume 3, edited by Frisch; the factors useful here are that a $\beta = 1$ charged particle passing through lucite produces approximately 240 photons/cm (in the photomultiplier frequency range) in a cone at 48° to the particle direction. Connections to the electronics were through 100-ft lengths of 197-Ω cable.

c. Magnetic Shielding. The counter location was subject to 450 gauss peak magnetic fields at full Bevatron magnet current. This necessitated extensive magnetic shielding for each of the photomultiplier tubes, particularly the 2-in. tubes used on the Cerenkov counter. The inner magnetic shielding for the 1P21 photomultiplier tubes consisted of two 1/16-in. concentric soft iron cylindrical shells around the phototube, with openings only slightly larger than the photocathode. The inner shielding for the RCA 6342 photomultiplier tubes was first 1/16-in. μ metal, then three concentric cylindrical iron shells ranging in thickness from 1/8 in. to 1/4 in. and extending beyond the photocathode some 4 in. The latter set of shells was machined to fit over the lucite light pipes on the Cerenkov counter and over part of the main lucite block. The lucite block was wrapped with aluminum foil, then covered with 1/16-in. μ metal sheet except for 2-by-2-in. particle entrance and exit; the cylindrical light pipes to the photomultiplier tube were similarly wrapped with permalloy tape. The Cerenkov lucite block was in turn surrounded by a soft iron box (3/4-in-thick walls) with openings only for particle entrance and exit and for the previous shielding around photomultiplier light pipes. Finally, as insurance, a large outer iron box 3/8-in.-thick walls) was installed around the entire counter telescope except for particle entrance and cable entrances. The assembly was tested under actual field conditions by monitoring the counting rate (during the magnetic cycle) for each of the counters exposed to a radioactive source but to no beam. A small sheet of plastic scintillation was used on the Cerenkov lucite block face for this test.

2. Collimation and Mounting

Since the counter telescope was to observe gammas, originating in limited regions of space, that are perhaps 10^{-4} times as intense as at the target, the collimation was extensive, as shown in Fig. 1. Specifically, the collimation was designed either to view a vertical shaft 1 by 1.75 in. with only slight 1^{o} geometrical fringing, or to view a shaft 0.5 by 1 in. with slightly larger fringing, the latter being

accomplished by slipping an insert into the second collimator from the target (this insert removed the edges of the first collimation aperture from the field of view). The collimation consisted primarily of four 2-in.-thick lead shields with apertures of 1 by 1.75 in., 1.5 by 2 in., 1.5 by 2 in. (or 0.5 by 1 in.), and 1 by 1.75 in. respectively from top (near counter) to bottom. (The thin dimensions were along the beam direction for better space resolution.) The relative locations for these apertures are shown in Fig. 1; the whole assembly is mounted as a rigid unit on an aluminum frame with the first and last collimation 52 in. apart and the lower two collimators on the aluminum frame projecting approximately 45 in. down into the north well of the west Bevatron tangent section.

A 3-in. lead block was pivoted by remote control in and out of the collimation aperture to act as a gamma shutter. The shutter was located on the top surface of the lowermost collimator, and allowed a correction to be made for pion charge-exchange scattering on the collimator surfaces and for wide-angled background from the machine (discussed in III-A).

The counter telescope and associated inner magnetic shielding were mounted as a rigid subunit on an aluminum frame; the outer magnetic shielding fitted over the telescope and the upper part of the frame. The collimation subunit was also attached to this frame below the level of the four wheels supporting the entire assembly on a track over the north well of the west tangent section. Two of the four wheels were geared to a long aluminum rod extension that could be operated from a safe location during machine operation for movement of the entire assembly along the beam direction. A pointer attached to the aluminum frame was read (against a scale fastened to the anchored rails) by use of an optical telescope viewed from the same location as the control rod termination.

C. Electronics

The electronics for this experiment had to meet the difficult requirement of making a logical analysis of events occurring within 2×10^{-8} second. The main component was a Garwin-Wiegand coincidence circuit[13] capable of performing a versatile set of decisions on 2- to 15-volt 5-millimicrosecond pulses. The possible decisions in this particular case were a sixfold coincidence, fourfold coincidence, and an answer stating that the fourfold ("Yes") but not the sixfold ("No") had occurred. This last function constitutes the "anti" feature of the circuit. A block diagram of the electronics is given in Fig. 4, showing the source of the sixfold and fourfold coincidences. The sixfold coincidence occurred for pulses of a charged particle in the front "anti" counter, defining counter, both arms of a Cerenkov counter, and rear counter. This of course provided both a "Yes" and a "No" output pulse. Note that the front counter pulses are first added together for high particle-detection efficiency for the electronic anti feature, and that the output of the amplified adder output is then used to feed two inputs on the sixfold coincidence to ease anticoincidence circuit requirements (i.e., a real gamma count thus gave a pulse in four out of six inputs instead of four out of five, virtually eliminating the difficulties of an "anti" circuit discriminating against the fourfold feed-throughs common to the later type of coincidence). Detected gammas passing through the front counter and converting to a pair in the converter gave pulses in the defining counter, in both arms of the Cerenkov counter, and in the back counter. This yielded output pulses in the "yes" and the "anti" categories.

The coincidence circuits and counter components were checked and plateaued on cosmic rays before runs on the Bevatron. The threshold for each of the coincidence circuits was checked daily through use of a 5-channel millimicrosecond pulser.

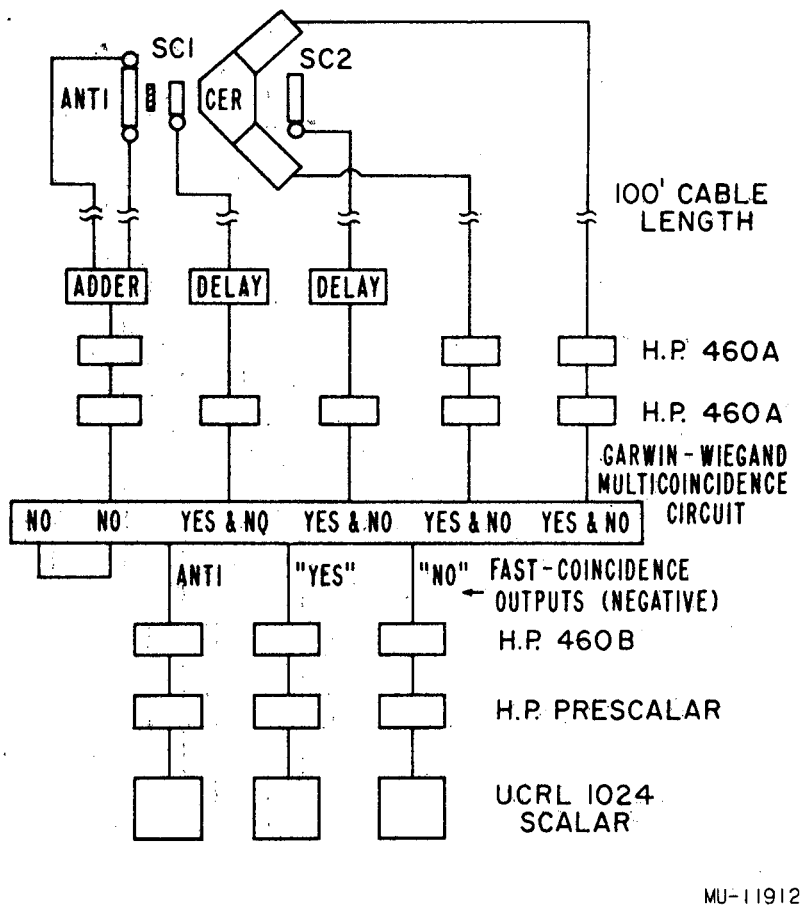

Fig. 4. Electronics block diagram.

1. Specific Components of the Electronics

a. Adder. The adder used to sum the two 1P21 photomultiplier tube outputs from the front anti counter is shown in Fig. 5. The pulses taken from this counter were the positive signals from the last dynode stage, and the adder acted also as an inverter for the negative pulse requirements of the coincidence circuits.

b. Fast Amplifiers. Commercial 460A Hewlett-Packard amplifiers were used to amplify the 5 μsec photomultiplier output pulses to a level near saturation for large pulses (over 4 volts for the average pulse) and hence acted as a limiter for the coincidence circuit inputs.

c. Multicoincidence and anticoincidence Circuit. The coincidence circuit used in this experiment was the Garwin-Wiegand type employing 404A tubes along a "distributed" Rossi coincidence circuit with a Garwin plate clamp.[13] Certain other refinements, such as the ability to change the number of coincidences from 1 to 6 by simple switch choices in each channel, have been added to make it an extremely versatile circuit. The thresholds for the multiple coincidence units were generally set at 1.5 to 2.0 volts. The anti feature was set to operate at a threshold near 2.2 volts for 5-μsec pulses. The circuit also contained a twofold circuit used for the pion-monitoring telescope. Each of the coincidence circuits gave three output pulses, namely, a fast 2-volt positive pulse, a 2-volt negative pulse, and a slower shaped 50-volt scaler pulse. The fast negative outputs were used here, each operating into a Hewlett-Packard 460-B amplifier, then to a Hewlett-Packard prescaler (which had been modified to allow gating), and finally into a UCRL 1024 scaler.

D. Monitor

The relative monitor used in this experiment consisted of two plastic scintillation counters, 1 in. in diameter and 0.5 in. thick, separated by a distance of 23 in., the front counter being 8 ft. 8 in. from the target and at 82° to the beam direction, as shown in Fig. 2.

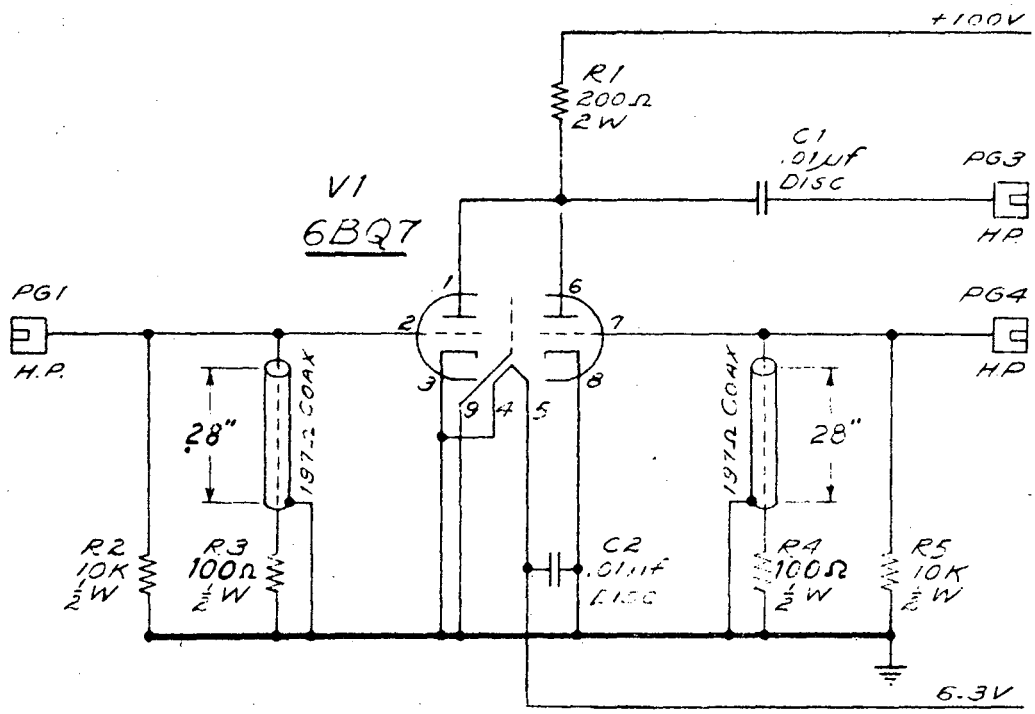

Fig. 5. Millimicrosecond pulse adder.

This form of monitor was chosen because it gives a reasonably accurate instantaneous record of the proton flux through the target, as it looks at charged-pion production occurring in the target. The induction electrode signal was used as a rough early relative calibration of the circulating beam, but for final analysis the pion telescope was calibrated by plunging a thin aluminum sandwich with the target. Since the cross section for aluminum spallation to Na^{24} was felt to be reasonably well known,[14] an absolute calibration was made by correlating the monitor counts against the Na^{24} activity in a 2-hour run with an aluminum sandwich (1-mil Al guard foil, 3-mil Al, 1-mil Al guard foil) covering the target face. This then corrected for multiple traversals and for beam missing the target, which are the sources of error in the circulating beam measurements. This method, on the other hand, introduces an appreciable absolute error (±20%) in the associated production cross sections given in V-B pending a better value of the cross section for aluminum spallation to Na^{24} (taken here as 9.3 mb for 6.0-Bev protons) and a better correction for evaporated neutrons producing Na^{24} (taken as a 15% correction for the 1/2-in. Cu target, 6% for the 1/8-in. Cu target).

III. COLLECTION AND TREATMENT OF DATA

A. Considerations for an Experimental Curve

For a given counter location the number of counts per monitor count represented, first of all, an integral over a space bit (determined by the collimation) along beam direction. This required the use of a "thin" target and narrow collimation for good space resolution. Moreover, to correct the raw gamma count obtained for background it was found necessary to make four runs for each position. These runs and their interpretation are as follows (the changes were done by remote control):

Condition		Interpretation
Converter in, shutter open	$\longrightarrow$	$N_{R\gamma}(c) + N_{R\gamma}(Pl) + N_{B\gamma}(c) + N_{B\gamma}(Pl) + A$
Converter out, shutter open	$\longrightarrow$	$N^0_{R\gamma}(Pl) + N^0_{B\gamma}(Pl) + A$
Converter in, shutter closed	$\longrightarrow$	$N^s_{B\gamma}(c) + N^s_{B\gamma}(Pl) + A^s$
Converter out, shutter closed	$\longrightarrow$	$N^{s0}_{B\gamma}(Pl) + A^s$

Here $N_{R\gamma} \equiv$ number of "real" gammas detected (from strange-particle decay),

$N_{B\gamma} \equiv$ number of "background" gammas detected (e.g., from pion charge-exchange scattering and π^0 production from neutrons), and

$A \equiv$ accidental counts (e.g. accidental pile-up of random background and the charged-particle counts because the "anti" counter is not a perfect detector; hence, to a good approximation not converter-sensitive).

The quantity of interest here is

$$(1-2)-(3-4) = N_{R\gamma}(c) + \left\{N_{R\gamma}(Pl) - N^0_{R\gamma}(Pl)\right\} + \left\{N_{B\gamma}(c) - N^s_{B\gamma}(c)\right\}$$
$$+ \left\{N_{B\gamma}(Pl) - N^0_{B\gamma}(Pl)\right\} - \left\{N^s_{B\gamma}(Pl) - N^{s0}_{B\gamma}(Pl)\right\} .$$

Here the first term, $N_{R\gamma}(c)$, represents the number of real counts of interest (converted in the lead converter; hence, appropriate to the counter calibration). The second term represents the number of

gammas ("real") converted in plastic scintillator (primarily Sc. 1) with the converter in, minus the number converting in the plastic with the converter out. Estimates of this difference between these small "correction" terms yield a correction of less than 5%. The third term represents the number of "background" gammas counted with the converter in minus a similar measurement with the 3-in. lead shutter closed. Since the principal source for these counts was the collimation surfaces, the estimated difference was negligible (the top of the shutter tended to compensate for the one obscured aperture surface). The last two terms were essentially zero, being very small differences of small correction terms (i.e., the quantities involved were very small and not very converter-sensitive). Hence, to a good approximation, $(1-2)-(3-4) \approx N_{R\gamma}(c)$, where we use the general notation $N_{R\gamma}(c) \equiv N_{\gamma}$.

Fortunately, the relatively small quantity (3-4) was essentially independent of position, which allowed an over-all averaging that reduced the statistical error contributed by (3-4) to the measurement of N_{γ}.

B. Slit Scattering and Target π^0 Contribution

Since the experimental curves were taken over positions upstream, on target, and downstream, there remained one major correction to the analysis of heavy-meson and hyperon decay. This was the gammas from the direct target production of π^0 mesons and the gammas scattered by the collimation apertures from this much more intense (target π^0) source of gammas. The solution here was to make a run from 0.8 to 1.0 Bev (below associated production threshold) to determine the effective slit resolution. The resolution was found to drop off sharply (as shown in Fig. 6) in an approximately symmetrical way, supporting previous threshold measurements to the limit of the sensitivity of our equipment. This experimental scattering measurement was applied at other energies simply by normalizing to the same on-target intensity, as the behavior of high-energy gammas was not expected to change in any very essential way, even though slight

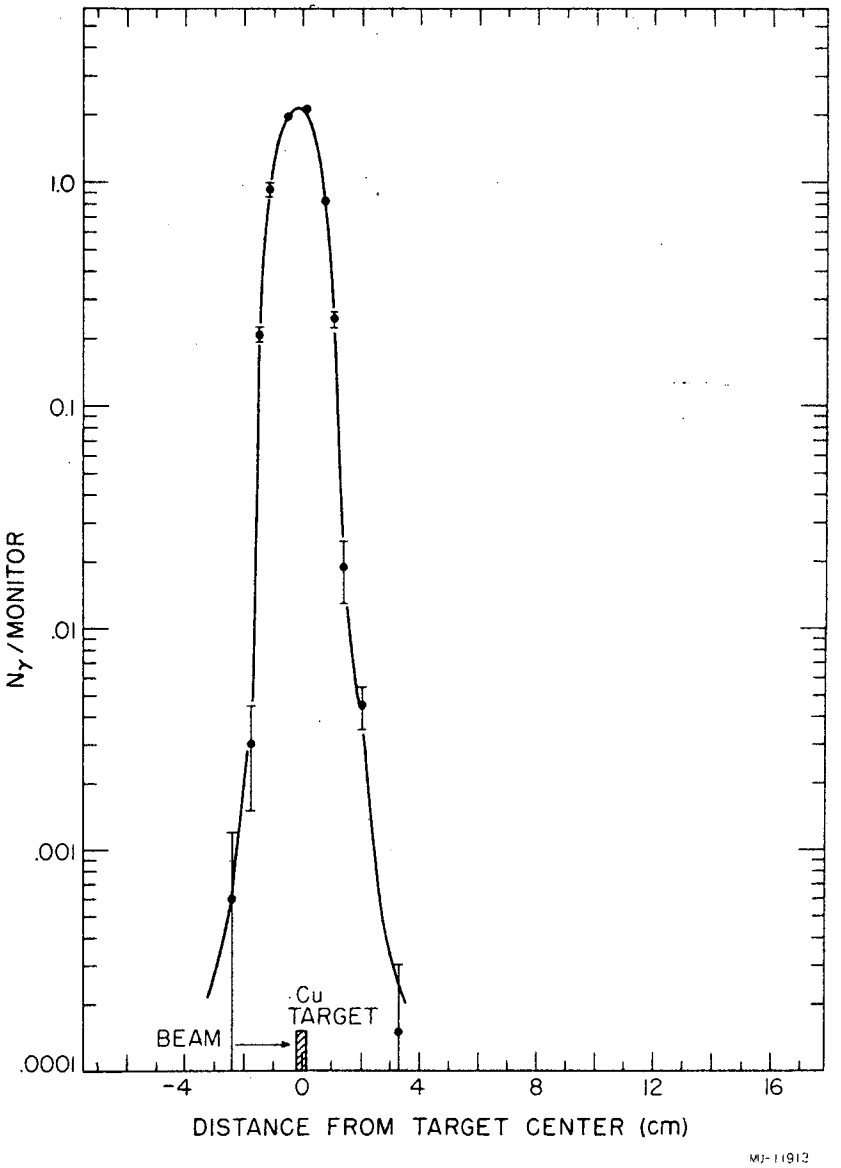

Fig. 6. Target π^0 contribution and slit scattering, 0.8 to 1.0 Bev, from 1/8-inch Cu target and 1/2-by-1-inch collimation.

changes were expected in the gamma spectrum at 90° with charges in Bevatron energy. (Dashed curves showing the extrapolated slit scattering are shown in Figs. 9 and 10.) It should be noted that though the statistical error of the resolution curve was large, the shape was felt to be reasonably well determined by additional checks. These were a repeat of a resolution curve for a similar slit, and agreement with the extrapolated upstream values, where checked on runs below 3.2 Bev. (the K contribution disappeared below 3 Bev, as it kinematically should).

IV. CONSIDERATIONS FOR A PREDICTED CURVE

A. Assumptions

The complete prediction for the expected spatial decay curves was based on the mechanics of $n + n \rightarrow n + Y + K$ (see I-B) and the subsequent possible decay modes of the Y and K particles. The mechanics (see Fig. 11a) first of all depends on the momentum and energies of the incident proton and of the struck nucleon. Then (in the center-of-momentum system) specific assumptions of the energy and angular dependence of the matrix elements involved must be made, and the three-body phase-space volume computed to give the probability distribution of energy division between the particles. Finally we must make a transformation to the laboratory system of the "cascade" two-body decay of the heavy meson or hyperon to π^0 mesons, and then to gammas. This is followed by folding in the calibrated counter efficiency (see VII-B) for the spectrum seen at 90° (lab) to determine the predicted decay curve as recorded by the counters.

The specific assumptions made were: (a) that the reaction was of form $n + n \rightarrow n + Y + K$, (b) that the incident-proton energy distribution was nearly linear from 5.7 to 6.2 Bev (as determined by viewing beam spill on an oscilloscope), (c) that the internal momentum distribution was a Fermi distribution with 24-Mev cutoff, (d) that for first trials the matrix element was to be constant and isotropic, (e) that an ordinary Fermi-model calculation of the phase space was made, and finally (f) that subsequent decays to π^0 mesons and to π^0 gammas were isotropic, on the basis of past experiments (the π^0 decay is of course isotropic, as the π^0 has spin zero). The tacit assumption is made throughout that pion modes of decay (and hence here via π^0) will predominate over direct electromagnetic modes unless largely forbidden for the particular unstable particle in question. Hence, essentially all gamma radiation seen was considered as coming from π^0 modes (except a possible contribution from Σ^0 decay very near the target), as the lifetimes accessible to this experiment were appropriate to the "stronger" form of coupling (slowed of course by $\Delta S = \pm 1$).

Calculations (discussed in VII) based on these assumptions were carried out with the aid of an IBM 650 digital computer.

On the basis of first trials, revisions were made in production angular dependence for a best fit of the upstream and downstream heavy-meson data, and in the energy dependence for a crude fit to a short sigment of the excitation curve.

B. Gamma-Counter Telescope Efficiency

The counter telescope was calibrated by a combination of experimental and theoretical methods.[10] The procedure was to experimentally determine the electron-counting efficiency of the counter telescope (without its front anti counter or regular lead converter) as a function of lead foil thickness (0 to 1/4 in.) in front of the counter, as a function of electron energy (30 to 300 Mev), and for various geometrical positions parallel to the telescope axis. This is in effect the simulation of a gamma conversion at a known position and depth in the converter into a known-energy electron. This electron-counting efficiency was folded in with the theoretical[15] probabilities of pair formation in the various elements of distance through the foil and with the theoretical energy-partition probabilities for the electron and positron pair.

The experimental setup (Fig. 7) involved the use of the Berkeley synchrotron bremsstrahlung beam to create a spectrum of electrons in a thin converter placed at the entrance of an analyzing magnet. A particular energy channel was selected by the field (and brief collimation) to pass through a beam-defining electron-monitoring telescope placed in front of the lead foils and counter telescope. The electron monitor consisted of two plastic scintillators 2/3 by 2/3 in. and 3/8 in. thick. This monitoring telescope defined the geometrical position of the electron beam of interest; it both activated a twofold coincidence for the electrons incident and also two inputs of a sixfold coincidence, where the other four inputs came from the counter telescope. This gave the electron-counting efficiency for the telescope, following lead of thickness x as:

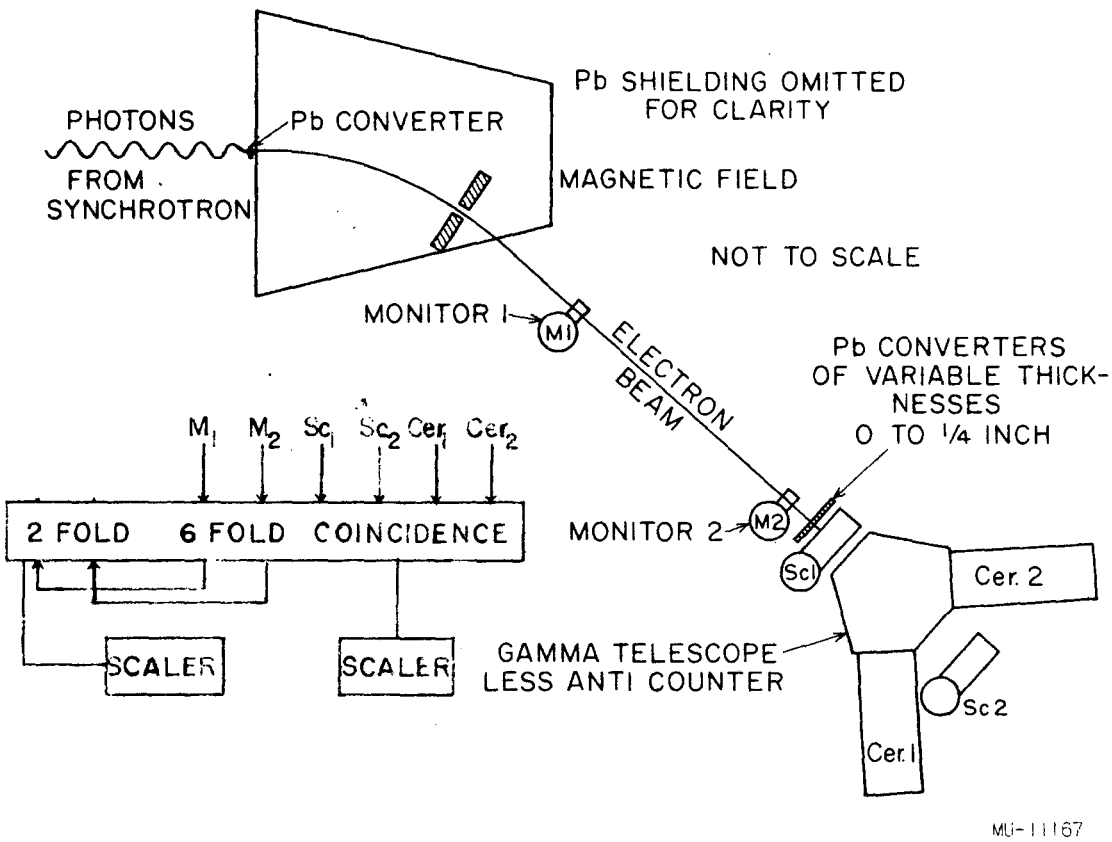

Fig. 7. Gamma-counter telescope calibration layout.

$$F(E, x) = \frac{\text{number sixfold}}{\text{number twofold}} \times 100\%$$

The geometrical effect was then averaged in, though it proved to be minor because the collimation used was small compared with the counter face.

Finally, to determine the gamma-ray counting efficiency for a gamma of particular energy, a numerical integration was performed using the calculated production of electron-positron pairs for different depths in the 0.196-in. converter for a gamma of this energy. Then the probability that an electron be produced with an energy E from this gamma at a distance x in the converter was multiplied by the experimental counting efficiency for recording a count from an electron of energy E incident on (0.196-x) inchs of lead before the telescope. The result(plus a similar contribution from the positron minus the probability that both the electron and positron gave a count) is given in Fig. 8. The accumulated errors in this determination give about a ±10% absolute error, though the relative error in the shape is believed small even in the extrapolated region of the curve given. The latter part of the curve was based on an extrapolation of experimental electron-counting efficiency in a very flat part of the curve; the main errors would therefore stem from an uncertainty in pair-production cross sections at these higher energies.

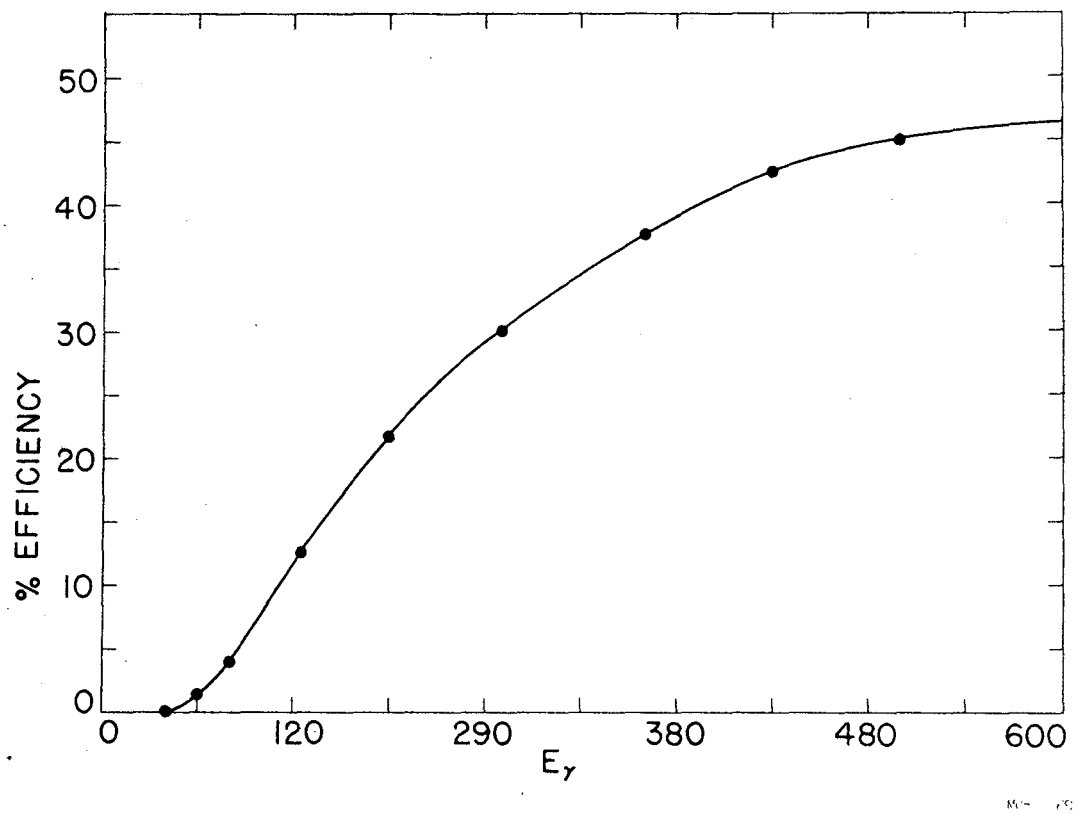

Fig. 8. Gamma-counter detection efficiency.

V. RESULTS AND DISCUSSION

A. Typical Corrected Curves

Experimental data corrected for background (discussed in section III-A, B) are given in Figs. 9 and 10. Figure 9 shows the data obtained at 5.7 to 6.0 Bev with a 1/8-in. Cu target and 0.5-by-1-in. collimation system. Figure 10 shows the data obtained from 5.7 to 6.2 Bev with using a 0.5-in. Cu target and 0.5-by-1-in. collimation. It should be noted that the fixed transverse collimation materially affects the apparent spatial slope of gamma intensity with distance (loss of diverging particles), but of course in a calculable way.

The dashed curves given in Figs. 9 and 10 represent the respective expected target π^0 contributions and slit-scattering contributions, as discussed in III-B.

B. Comparison with Calculated Curves

The results of calculations based on assumptions of matrix-element dependence of $/H/^2 \propto \left\{\frac{E_\theta^2}{M_\theta^2} - 1\right\} \mathrm{Cos}^{14}\theta$, and two-pion heavy-meson decay (at least one π^0) as seen through the collimation and detected by the counter telescope at 90° are given as dashed lines in Figs. 9a and 10a. The upstream data and first section downstream yield agreement with a K meson decaying through two pions (at least one π^0) with a mean lifetime of $1.9^{+.2}_{-.3} \times 10^{-10}$ sec. The second downstream section can be roughly fitted by adding (to the θ^0 contribution) either a hyperon decaying into π^0 and nucleon with a mean lifetime of near 4×10^{-10} sec (i.e. $\Lambda^0 \rightarrow n + \pi^0$), or a contribution from $\theta + \rightarrow \pi^0 + \pi^+$ or both. The data near 6.0 Bev appear to be insufficient to separate these two possibilities, and the fit further implies other forms of production where the resulting strange particles have little energy in the c.m. system. The latter type of production would give the low loss by particle divergence in the laboratory system necessary to fit the nearly flat curve of experimental data from far downstream, and could include associated production involving additional pions as observed by Fowler.[4]

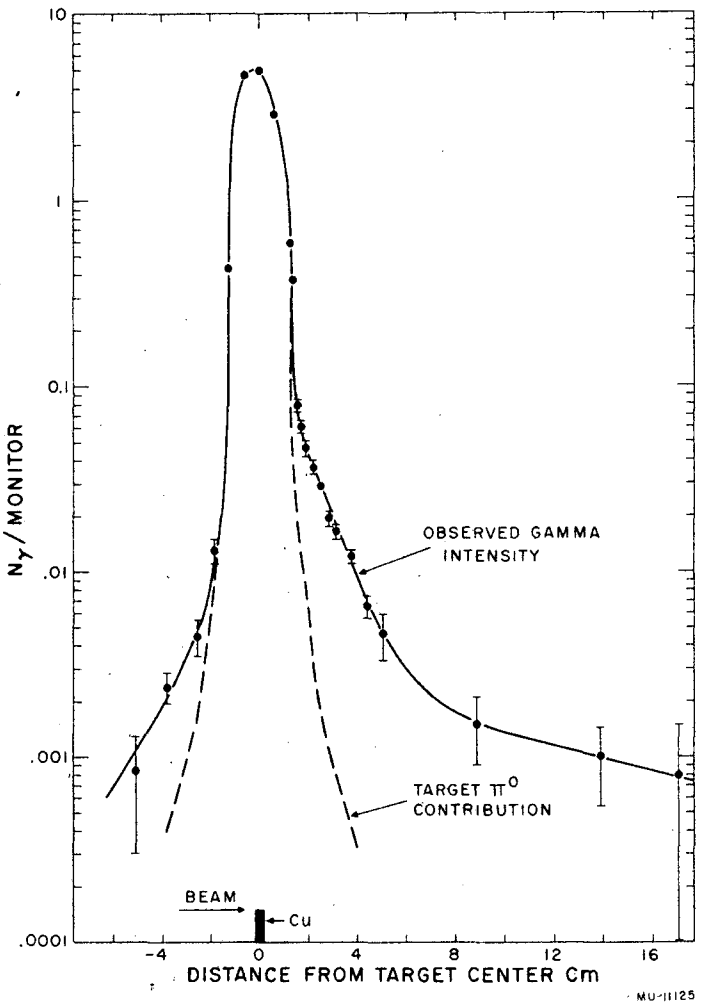

Fig. 9. Experimental data for π^0 modes of heavy-meson and hyperon decay; 5.7- to 6.0-Bev protons incident on a 1/8-inch Cu target, viewed with the 0.5-by-1-inch collimation aperture.

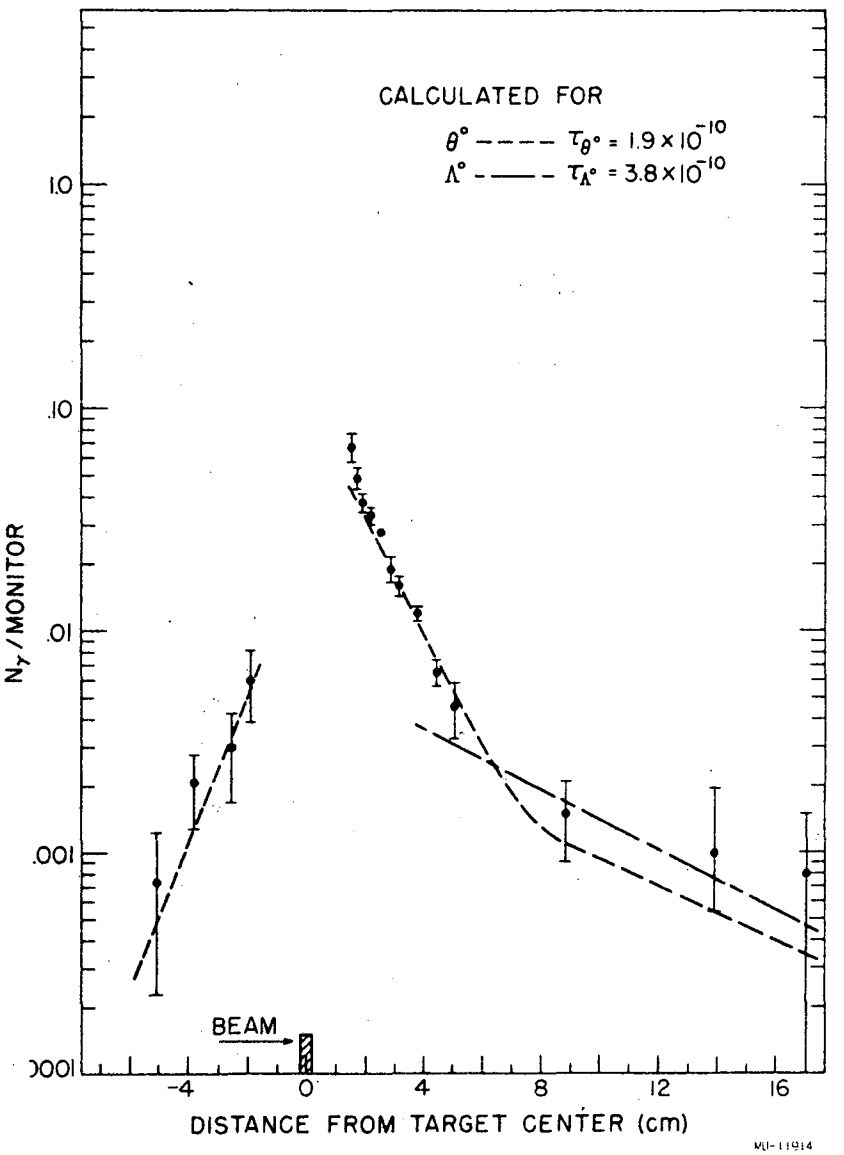

Fig. 9a. Calculated curves for θ^0 decay and Λ^0 decay compared with the experimental data of Fig. 9. The θ^0 and Λ^0 curves were calculated for equal cross sections and matrix element energy and angular dependences of $|H|^2 \propto \{E^2/M^2 - 1\} \cos^{14}\theta$ in the c.m. system, where E, M, θ refer to the particular particle in question.

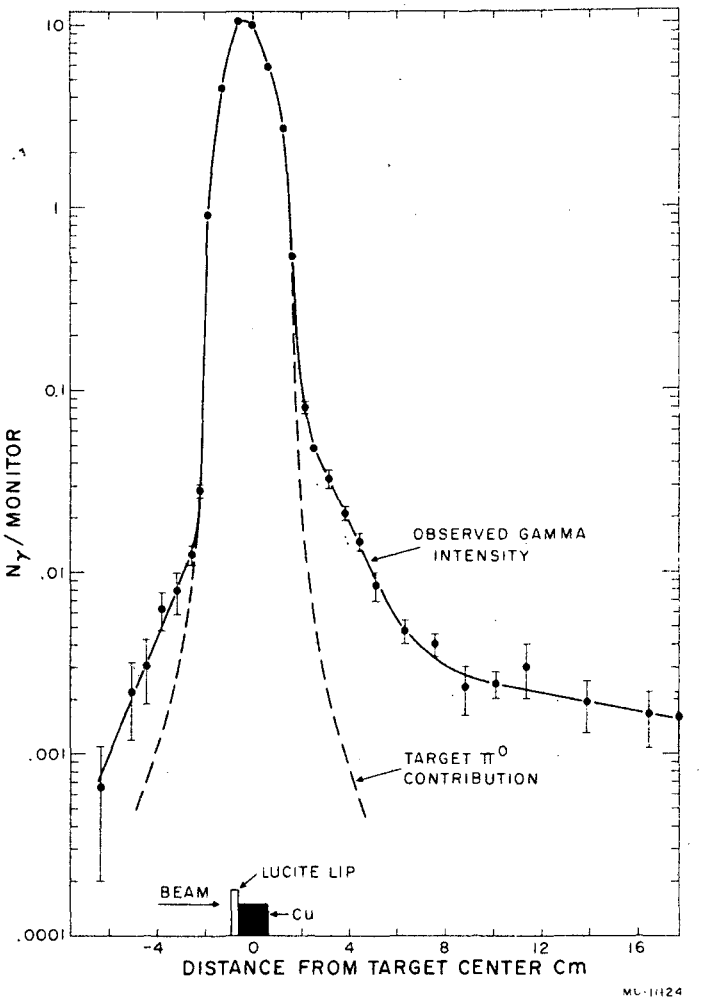

Fig. 10. Experimental data for π^0 modes of heavy-meson and hyperon decay; 5.7- to 6.2-Bev protons incident on a 0.5-inch Cu target, viewed with the 0.5-by-1-inch collimation aperture.

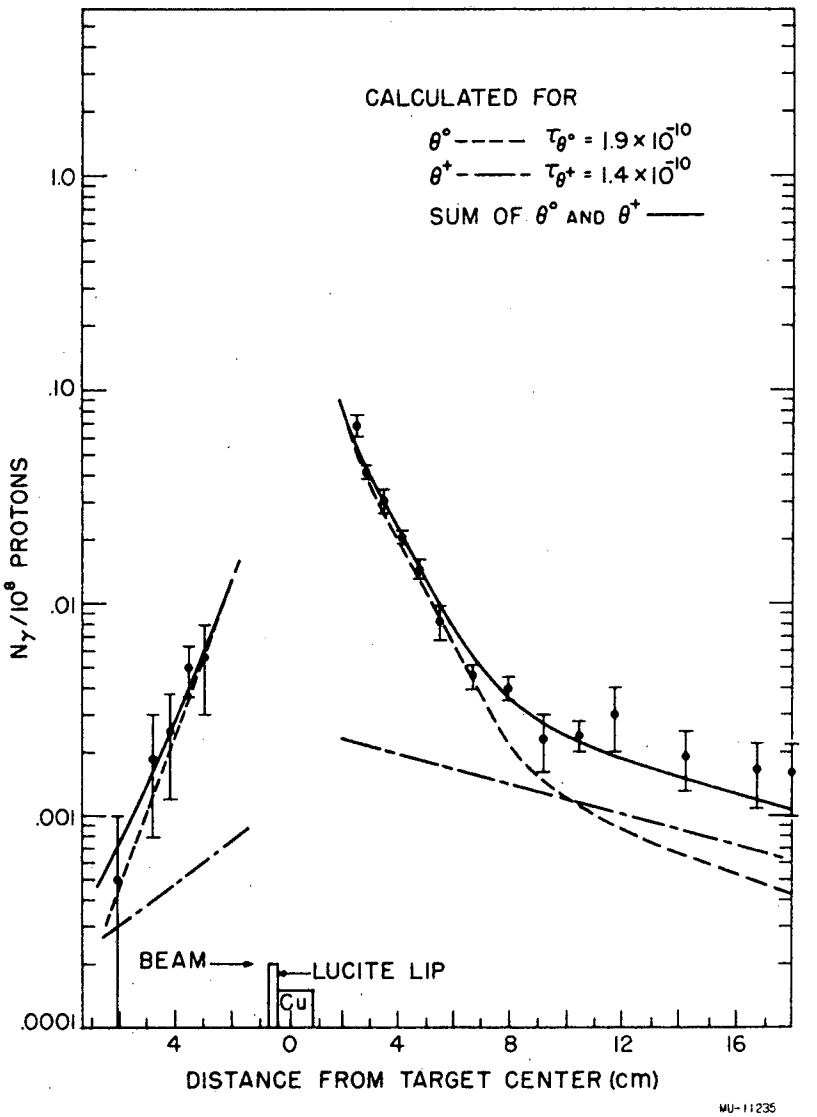

Fig. 10a. Calculated curves for θ^0 decay and θ^+ decay compared with the experimental data of Fig. 10. The θ^0 and θ^+ curves were calculated for equal cross sections and matrix-element energy and angular dependences of $|H|^2 \propto \langle E^2/m^2 - 1 \rangle \cos^{14}\theta$ in the c.m. system, where E, m, θ refer to the particular particle in question.

The matrix-element dependence on energy and production angular distribution was determined by a best fit to the experimental data. First of all the production angular distribution of the heavy meson was varied for a best fit for the relative amount of the heavy-meson upstream and downstream contributions. This proved to be very sensitive to the angular distribution and only slightly dependent on the $/H/^2$ energy dependence and on lifetime. The lifetime, however, was not an entirely free parameter; it was largely determined by the spatial slopes, but the slopes, in turn, are slightly influenced by the angular distribution. A best fit for the data for 5.7 to 6.2 Bev was given by $\cos^{14}\theta$. The energy dependence was explored by comparing calculated and experimental curves at both 4.8 to 5.3 Bev and 5.7 to 6.2 Bev, on the assumption of a similar angular distribution with a slightly better (not very sensitive) fit for $\left\{E_\theta{}^2/M_\theta{}^2 - 1\right\}$.

C. Discussion and Conclusions

The fit to known particles follows directly for the K meson, since we can interpret the data as $\theta^0 \rightarrow \pi^0 + \pi^0$, with $\tau_\theta{}^0 = 1.9^{+.2}_{-.3} \times 10^{-3}$ sec mean lifetime. Since this decay mode is into two identical spinless bosons, the θ^0 must have even spin and positive parity. This interpretation appears quite unambiguous, as no other known K^0 or K^+ has a lifetime near this range; however, there is a current disagreement as to the mean lifetime of the θ^0. Namely, a number of experiments (including this work) gave a mean lifetime near 1.7×10^{-10} sec, while several recent cloud-chamber experiments gave a mean lifetime of approximately 0.60×10^{-10} sec.[16] I believe that the difference is due to some systematic error, though the possibility of another shortlived K cannot be completely discounted.

The cross section per nucleon (for protons at 5.7 to 6.2 Bev) for associated production as seen through $\theta^0 \rightarrow \pi^0 + \pi^0$ was $0.22 \pm .07$ mb under the assumptions of V-B. This cross section, when compared with the rough cross section for associated production (no good data available for nucleon-nucleon collisions at the energies used) seen

through $\theta^0 \rightarrow \pi^+ + \pi^-$ in cloud-chamber work, yields a branching ratio for $\frac{\theta^0 \rightarrow \pi^0 + \pi^0}{\theta^0 \rightarrow \pi^+ + \pi^-}$ on the order of 1. Unfortunately a more accurate value for this is needed for extracting full theoretical significance.[17, 18, 19]

The very marked angular distribution found for heavy-meson production requires strong contributions for angular momenta $L = 7 \pm 1$ in the usual partial-wave picture. This finding seems somewhat surprising, but possibly not at variance with current models of multiple meson production. A simplification would result if the spins of some of the strange particles were higher than currently expected, since it is $\vec{L} + \vec{S}$ that is conserved in the reaction. An alternate line of thought requiring a peaked angular distribution would be that for a "compound nucleon" picture, wherein associated production might be thought of as a stripping reaction of a nucleon into a K + Y, the K going on forward. (Either the incident or struck nucleon could strip, making the reaction symmetric in the c.m. system.) On the other hand, certain aspects of the data, such as the apparent appreciably upstream K-meson energy in the laboratory system and disappearance of the upstream K contribution near 3 Bev, do not easily fit into the stripping picture unless there are additional contributions from a localized strong interaction. The same problem of strong forward peaking appears to occur also in $\pi^- + p \rightarrow \Lambda^0 + \theta^0$, and K^+ "scattering."

The presence of other particles is also implied by the data, but not in an unambiguous way; namely, the data near 15 cm downstream would be consistent with contributions from either or both $\Lambda^0 \rightarrow n + \pi^0$ and $\theta^+ \rightarrow \pi^+ + \pi^0$. The occurrence of $\theta^+ \rightarrow \pi^+ + \pi^0$ is also implied more specifically (but with poor statistics) by upstream data taken for protons of 4.8 to 5.3 Bev. In this case the θ^0's decay very rapidly, owing to low laboratory energies (and little time dilation), while the θ^+ has a 1/e distance, which becomes more appropriate to the counter geometry. In addition, the break to a steeper slope observed from the data very near the target downstream is possibly appropriate to a contribution from $\Sigma^+ \rightarrow \pi^0 + p$. Specifically designed

experiments are planned for a later date to resolve these three possible contributions and to determine the branching ratio of the θ^0 by observing the charged decay products.

The lifetime determination and angular distributions require a statement of qualification, though the correction is felt to be relatively small.

(a) A Fermi internal-momentum distribution for the struck nucleon was chosen for simplicity over a perhaps more realistic gaussian distribution. The effect was estimated (and approximately checked) to be very slight.

(b) A matrix-element energy dependence stronger than the $\left(E_\theta{}^2/M_\theta{}^2 - 1\right)_{c.m.}$ used would allow slightly weaker angular dependence and shorter lifetimes; however, the excitation function appears too flat to allow a stronger energy dependence than the preliminary fit given. The possibility of a higher power of the term $\left(E_\theta{}^2/M_\theta{}^2 - 1\right)$ will be carefully checked when the work on the excitation function is completed.

(c) The three-body phase-space factor used conserved only total energy and momentum, and since high angular momenta are apparently involved, the conservation of $\vec{L}$ is not trivial. The correction due to this factor would again tend toward less pronounced angular dependence and shorter mean lifetime, and is felt to be the most significant correction. Owing to the difficult calculations involved no estimated correction has yet been applied.

(d) The decay process of the θ^0 may not be isotropic though cloud-chamber data indicate that it is very nearly isotropic and unpolarized; hence, the effect is probably very slight.

(e) Other reaction mechanisms, such as discussed in Section I-B (also including prominently $n + n \rightarrow n + Y + K + \pi$, undoubtedly make some contribution to the data. However, the large upstream contribution and relatively large counting rate near the target indicate rather clearly that the dominent kinematics are appropriate only to a three-body final state such as the form $n + n \rightarrow n + Y + K$ used here. No

correction to this basic form has been applied; the evidence that this is small seems good, but no specific limit can be set from these data.

A similar experiment[20] has been performed at the Cosmotron by Collins and Ridgeway. Their experiment was done near threshold, yielding data with a spatial decay rate consistent with that reported here; the analysis is incomplete.

ACKNOWLEDGMENTS

I would like to thank the many people at the Radiation Laboratory who have aided in completing this experiment, particularly Professor Burton J. Moyer for this helpful advice and encouragement. Special mention is also due Dr. Robert Squire and Sherwood Parker for their parts in the early development and later instrumentation (and operation), respectively.

I wish also to extend my thanks to the computing departments of the Radiation Laboratory and Livermore Laboratory and particularly to Robert Pexton and Don Freeman for their time spent in programming and carrying out the lengthy computations involved.

Finally, thanks are due Dr. Edward Lofgren and the members of the Bevatron crew for the operation of the Bevatron.

This work was done under the auspices of the U. S. Atomic Energy Commission.

APPENDIX

A. General Definitions for Symbols used in Appendix

E = total energy (Mev.)

P = pc "momentum" (i.e., p units $\frac{\text{Energy}}{c}$)

T = kinetic energy

M = mc^2 (M refers to nucleon "mass" unless specified)

N = total energy in center-of-momentum (c.m.) system

β = velocity/speed of light (c)

$\gamma = \frac{1}{\sqrt{1-\beta^2}}$

T_0 = kinetic energy of incident proton

P_0 = "momentum" of incident proton

T_F = kinetic energy of struck nucleon

P_F = "momentum" of struck nucleon

μ = projected β of struck nucleon (along x axis)

$M\mu$ = projected momentum of struck nucleon (along x axis)

θ_F = angle between $\vec{P}_0$ and $\vec{P}_F$

E_T = total energy of system; P_T = total "momentum of system"

θ_K = polar angle of emission for K meson

ϕ_K = azimuthal angle of emission for K meson

E_K = total energy of K meson

E_Y = total energy of Y hyperon

E_n = total energy of final-state nucleon

P_K = "momentum" of K

P_Y = "momentum" of Y

P_n = "momentum" of final-state nucleon

Θ = angle between K meson and subsequent γ (in lab system).

$E_0^{\gamma} = M_{\pi^0}/2$; E_γ = γ energy

x_L = (+) coordinate along beam direction from target (lab system).

Note: In use in the text a second subscript is added, which indicates reference frame. These are L for lab, C for c.m., and K for K frame (e.g., P_{0L} = incident-proton "momentum" in lab system).

B. Useful Relativistic Relations

$$E_{lab} = \gamma_{c.m.} (E_{c.m.} + \beta_{c.m.} P_{c.m.} \cos\theta_{c.m.})$$

$$P_{lab} \cos\theta_{lab} = \gamma_{c.m.} (P_{c.m.} \cos\theta_{c.m.} + \beta_{c.m.} E_{c.m.}),$$

and $$P_L \sin\theta_L = P_{c.m.} \sin\theta_{c.m.}$$

$$\tan\theta_{lab} = \frac{P_{c.m.} \sin\theta_{c.m.}}{\gamma_{c.m.} (P_{c.m.} \cos\theta_{c.m.} + \beta_{c.m.} E_{c.m.})}; \quad \phi_{lab} = \phi_{c.m.}$$

$E^2 - P^2$ = invariant for a particle or system of particles.

$P^2 = T(T+2M)$ and $E^2 - P^2 = M^2$ for a particle.

$\beta = \frac{P}{E}$ for a particle or system of particles.

$\gamma = \frac{E}{\sqrt{E^2 - P^2}}$ for a particle or system of particles.

C. Kinematics

The method of presentation for the calculation of the kinematics follows: first, a brief step-by-step outline of the line of analysis used; secondly, a statement of notation (above) and general relations assumed; and finally, a detailed presentation of each step.

1. The kinematics logically starts with a consideration of the incident-proton and struck-nucleon momenta. From these the velocity of the center-of-momentum system (c.m.) and the total energy available in the c.m. system can be calculated.

2. Then a model of the reaction in the c. m. system must be assumed (e. g., $p + n \rightarrow n + Y + K$).

3. In the reaction energy and angular dependence for a matrix element ($/H/^2$) must be assumed for trial calculations and be fit, if possible, to experimental data. Also, in the reaction, the phase-space factor (in this case three-body relativistic) must be calculated to get the energy spectrum of any one of the particles.

4. This then allows a calculation of the probability that one of the particles (say, for the purpose of discussion, the K meson) is emitted in a particular $(\Delta\Omega)_{\theta, \phi}$ with energy E (E to E+Δ E) in the c. m. system. Since the velocity of the c. m. system is known, there is a specific transformation for $(\theta, \phi, E)_{c.m.}$ to $(\theta, \phi, E)_{lab}$. Knowledge of the c. m. quatity specifies the probability of finding a K meson in a specific element of "volume" (θ, ϕ, E) in the c. m. system; knowledge of the lab quantities is required to determine, first of all, if this particular group is in the field of view of the counter telescope $(f(\theta, \phi, x)_{lab})$, and secondly, the probability of decay for members of this group within the field of view $(g(\theta, E, x, \tau)_{lab})$ of the telescope.

5. For the K meson that does decay, a specific choice of decay mode must be considered (e. g., $\theta^0 \rightarrow \pi^0 + \pi^0$). Fortunately the assumption of isotropic decay for both θ^0 and π^0 permitted a marked simplification in the transformation of the gamma spectrum in the laboratory system.

6. This spectrum then was folded with the counter-telescope detection efficiency to yield the probability of a count.

7. Finally, the integrand made up of the probability of the K meson's being emitted in an appropriate $(\Delta\Omega, E)_{c.m.}$, times the probability of its decaying from x to x +Δ x, times the probability of detection of a resultant gamma ray, must be summed over available values of $(\theta, \phi, E)_{c.m.}$, subject to limits enforced by the collimation. This quantity must in turn be corrected for the variation in incident-proton energies, the spectrum of struck-nucleon momenta, and the target thickness, and finally be integrated over x for the space bite viewed by the counter telescope.

The detailed expansion of each step follows with algebraic manipulations merely outlined. Sketches of the reaction kinematics are shown in Fig. 11.

1. The incident-proton kinetic energy T_{0L} was determined by reference to Bevatron magnet-current markers triggered for specific magnetic fields and hence related proton energies. The induction-electrode signal (which monitors circulating beam) was simultaneously displayed on an oscilloscope to show the relative amount of beam striking the target per energy interval during the beam spill-out. The normal spill-out was essentially linear, though variations did occur.

The internal momentum distribution for the nucleons in the copper nuclei (Cu target) was taken, for simplicity, as the Fermi model. Namely,

$$N(P_{FL})dP_{FL} \propto P^2_{FL}dP_{FL} \text{ for } P_{FL} \leq P^{max}_{FL},$$

$$\text{and} = 0 \text{ for } P_{FL} > P^{max}_{FL}.$$

Making the substitution $P_x \equiv P_{FL} \cos \theta_{FL}$ and integrating over the range of θ_{FL} available, one obtains the form

$$N(P_x)dP_x = A(1-BP_x^2).$$

Changing notation to conform with the work of Block, Harth, and Sternheimer,[21] one gets

$$N(\mu) = 3.4 - 67.9\mu^2,$$

$$\text{where } \mu \equiv \beta_x \ (\mu = \pm 0.22 \text{ at cutoff}),$$

$P_x \equiv M\mu$, and $N(\mu) \equiv$ density of nucleons with projected velocity μc.

With a particular choice of $\vec{P}_{0L}$ and $\vec{P}_{FL}$ one can calculate the quatities of interest, such as the velocity of the c.m. system and the total energy available in the c.m. system (denoted by N). Since $\sqrt{E^2 - P^2}$ is an invariant,[22] we have

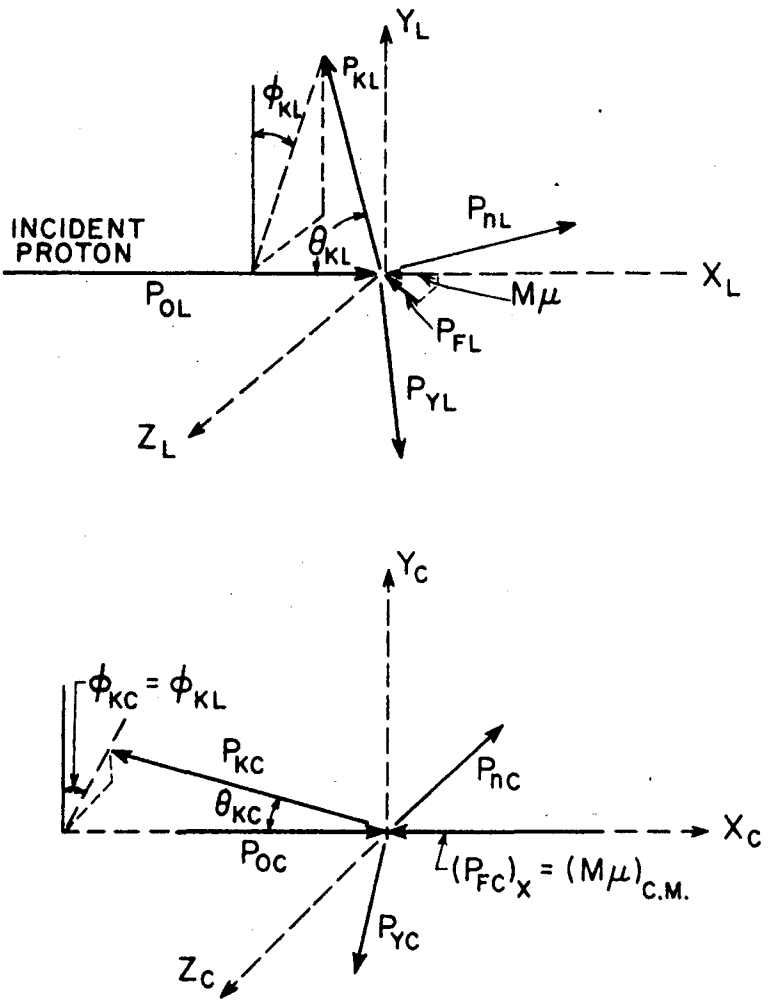

Fig. 11. Typical production schematic for p+n→n+Y+K (following K). Above: laboratory system. Below: center-of-momentum system.

$$N \equiv \sqrt{E^2_{TL} - P^2_{TL}},$$

where we note from below that $E_{TL} = (T_{OL} + M) + (T_{FL} + M)$

and $P^2_{TL} = P^2_{OL} + P^2_{FL} + 2P_{OL} P_{FL} \cos\theta_{FL}$.

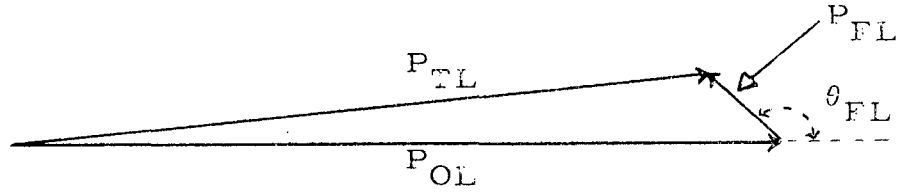

Therefore

$$N = \sqrt{\left\{T_{OL} + T_{FL} + 2M\right\}^2 - P^2_{OL} - P^2_{FL} - 2P_{OL} P_{FL} \cos\theta_{FL}},$$

but, since $T_{FL} << T_{OL} + 2M$, $P^2_{FL} << P^2_{OL}$, and $T_{FL} < M$,

$$N \approx \sqrt{(T_{OL} + 2M)^2 - P^2_{OL} - 2P_{OL} P_{FL} \cos\theta_{FL}}.$$

Also $P^2_{OL} = T_{OL}(T_{OL} + 2M)$ and $P_{FL} \cos\theta_{FL} = M\mu$,

therefore we can write

$$N \approx \sqrt{(T_{OL} + 2M)\,2M - 2\sqrt{T_{OL}(T_{OL} + 2M)}\,M\mu}.$$

This functional form of N reduces the dependence on the internal momentum of the target (to a good approximation) to involve only the influence of the projected "momentum" $M\mu$.

Similarly,

$$\beta_{c.m.} \equiv \frac{P_{TL}}{E_{TL}} = \frac{\sqrt{T_{OL}(T_{OL} + 2M) + P^2_F + 2\sqrt{T_{OL}(T_{OL} + 2M)}\,M\mu}}{T_0 + T_F + 2M},$$

and since $P^2_{FL} << P^2_{OL}$ and $T_{FL} << 2M$, we can write

$$\beta_{c.m.} \approx \frac{\sqrt{T_{OL}\,(T_{OL}+2M)}}{T_{OL}+2M} = \sqrt{\frac{T_{OL}}{T_{OL}+2M}} \equiv \bar{\beta}\,.$$

Similarly, we have

$$\gamma_{c.m.} \approx \sqrt{\frac{T_{OL}+2M}{2M}} \equiv \bar{\gamma}\,,$$

where, to a good approximation, the quantities $\bar{\beta}$ and $\bar{\gamma}$ used here are independent of the internal momentum distributions.

2. The question of reaction model was covered under I-C, with $P+n \rightarrow n+Y+K$ taken as the basic reaction (n ≡ nucleon). For this form, strangeness conservation requires that the K be limited to K^+ or K^0; the Y limited to Λ^0 or $\Sigma^{\pm,0}$. In the laboratory system one might conceive of the reaction shown in Fig. 11, where the K and Y in turn decay into products possibly including the π^0 mesons of interest here, and the π^0 of course decay rapidly to two gammas (99% of π^0 decays).

3. The basic characteristics of the reaction in the c.m. system consists of the $|H|^2$ energy and angular dependence and the phase-space factor. The method used for $|H|^2$ was to perform the calculations with a simple picture of no energy dependence and an isotropic angular distribution, and then essentially repeat, allowing variations of the form $\left(E^2_{KC}/M^2_K - 1\right)^k$ and $\cos^j \theta_{KC}$ until a reasonable fit to the data was obtained. A preliminary fit to the energy dependence was made on the basis of a short segment of the excitation function, while the angular dependence was simultaneously varied to give a reasonably sensitive fit to the upstream and downstream K-meson data.

The three-body relativistic phase-space factor is needed to give the shape of the energy spectrum of any of the three particles involved. In the following derivation of the spectrum shape, particular attention is given to the K meson; however, by an appropriate permutation of subscripts the derivation could be applied to any of the particles. The model used here was the simple Fermi model[23] conserving N and $\vec{P}$; the conservation of $\vec{L}$ was neglected owing to the difficult calculations required and the feeling that many angular momentum states could be

involved at such high energies that this would tend to cancel out any effect. It would appear that some correction should be applied to this approximation, as subsequent analysis indicates large values of L are dominant. The Lepore-Neuman[24] phase-space model was considered more realistic (it decreased high-energy components slightly); however, it was not used because of its more difficult form and the approximation of not accounting for $\vec{L}$ conservation in either case. The method used was as follows for the assumed reaction $p+n \rightarrow n+Y+K$. In "momentum" space using c.m.-system quantities we have

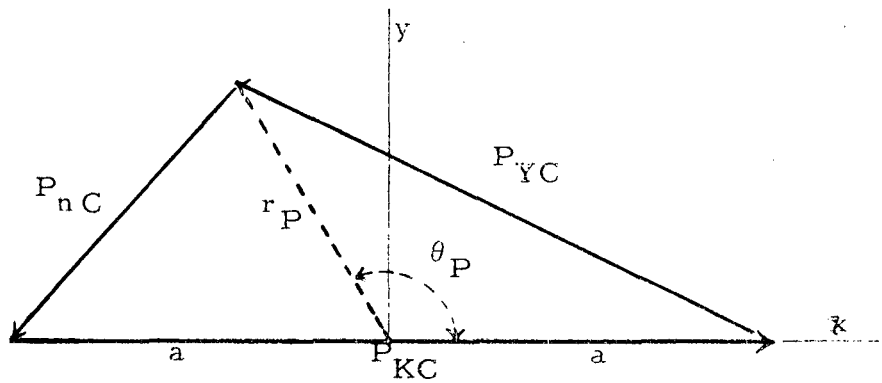

By energy conservation, we have

$$N = \sqrt{M^2_{KC} + P^2_{KC}} + \sqrt{M^2_{YC} + P^2_{YC}} + \sqrt{M^2_{nC} + P^2_{nC}},$$

and by P conservation,

$$\vec{P}_{KC} + \vec{P}_{YC} + \vec{P}_{nC} = 0.$$

Further, the following substitutions were made to automatically account for $\vec{P}$ conservation:

$$\vec{P}_{KC} = 2a\hat{i},$$

$$\vec{P}_{YC} = (x-a)\hat{i} + y\hat{j}$$

$$\vec{P}_{nC} = -(x+a)\hat{i} - y\hat{j}.$$

For ease of evaluation the substitutions $x = r_P \cos\theta_P$ and $x^2 + y^2 = r^2_P$ were made. Here r_P has the geometrical value shown in the above figure, and the physical interpretation that r_P represents the radius in phase space of the shell traced out by the vertex of P_{YC} and P_{NC} as they vary--(subject to the above limitations conserving N and $\vec{P}$; they of course can also rotate about the x axis). The volume contained within the shell in phase space divided by $(2\pi\hbar)^3$ represents the number of states available. The volume in momentum space was then evaluated, with P_{KC} held fixed:

$$V = \int_0^{\pi} \int_0^{r_P} 2\pi r^2 \sin\theta_P \, dr \, d\theta_P = \pi/6 \, \frac{(N-E_{KC}) \left\{ \right\}^{3/2}}{\left[(N-E_{KC})^2 - P^2_{KC}\right]^2},$$

where

$$\left\{ \right\} \equiv \left\{ (M^2_Y - M^2_n)^2 - 2\,(M^2_Y + M^2_n)\left[(N-E_{KC})^2 - P^2_{KC}\right] + \left[(N-E_{KC})^2 - P^2_{KC}\right]^2 \right\}.$$

Now the phase-space factor consists of the density of final states for a particular N available; hence, we need to evaluate $\partial V/\partial N$:

$$\frac{\partial V}{\partial N} = \pi/6 \left\{ 1 - \frac{2(M^2_Y + M^2_n)}{(N-E_{KC})^2 - P^2_{KC}} + \left[\frac{N^2_Y - M^2_n}{(N-E_{KC})^2 - P^2_{KC}}\right]^2 \right\}^{1/2} \cdot \left\{ 3\,(N-E_{KC})^2 \cdot \left[1 - \left(\frac{M^2_Y - M^2_n}{(N-E_{KC})^2 - P^2_{KC}}\right)^2\right] - P^2_{KC} \left[1 - \frac{2\,(M^2_Y + M^2_n)}{(N-E_{KC})^2 - P^2_{KC}} + \left\{\frac{M^2_Y - M^2_n}{(N-E_{KC})^2 - P^2_{KC}}\right\}^2\right] \right\}$$

$$\text{and } \frac{\partial N_K}{\partial P_{KC}} = \frac{4\pi P^2_{KC}}{(2\pi\hbar)^6} \frac{\partial V}{\partial N},$$

$$\text{or } \frac{\partial N_K}{\partial P_{KC}} = \frac{4\pi P_{KC} E_{KC}}{(2\pi\hbar)^6} \frac{\partial V}{\partial N} \equiv F(N, E_{KC}),$$

Where N_K refers to the number of K-Meson States. This factor $F(N, E_{KC})$ then gives the probability distribution of energies for the K meson (or Y hyperon, or n nucleon with appropriate index changes) in the center-of-momentum system, subject to the approximation that $\vec{L}$ is not explicitly conserved.

4. With the above factor F and a specific assumed energy and angular dependence of $/H/^2$, the probability of a K meson's being emitted in $d\Omega$, dE in the c.m. system for a particular associated production event is determined. The probability of being emitted in $d\Omega)_{\theta_{KC}}$ can be written as

$$\frac{\cos^j \theta_{KC}\, d\Omega_{KC}}{\iint \cos^j \theta_{KC}\, d\Omega_{KC}},$$

on assumption of axial symmetry (case j = 0, isotropic). The probability of being emitted in $dE)_{E_{KC}}$ can be written as

$$\frac{F(N, E_{KC}) \left\{ \frac{E^2_{KC}}{M^2_K} - 1 \right\}^k d E_{KC}}{\int F(N, E_{KC}) \left\{ \frac{E^2_{KC}}{M^2_K} - 1 \right\}^k d E_{KC}}$$ (case k = 0, no energy dependence).

The product of these two factors for a particular choice of j and k then yields the probability of the K meson's being emitted into the "volume" element $(d\Omega_{KC}, dE_{KC})$ having coordinates θ_{KC}, ϕ_{KC}, E_{KC}. Having chosen a set of values of θ_{KC}, ϕ_{KC}, E_{KC}), we have specific relativistic transformation to a corresponding set $(\theta_{KL}, \phi_{KL}, E_{KL})$. It is knowledge of the latter set of quantities and of the x coordinate, that allows a statement of whether the K meson can pass through the field of view, and also the probability that it decays while in the field of view of the counter. (The question of the limits on the K meson such that it can pass within the field of view is discussed in Section 7.) The projected laboratory-system spatial decay rate at x of a K meson with a mean lifetime τ_K, a velocity $\beta_{KL}\, c$, and at an angle θ_{KL} is given by

$$\frac{\exp\left(-\dfrac{x}{\beta_{KL}\,\gamma_{KL}\,c\tau_K\cos\theta_{KL}}\right)}{\beta_{KL}\,\gamma_{KL}\,c\tau_K\cos\theta_{KL}}$$

This results from the usual spatial decay rate, since we have

$t_{KK}\,(\text{time}) = \dfrac{t_{KL}}{\gamma_{KL}}$, $t_{KL} = \dfrac{D}{\beta_{KL}\,c}$, and $D = \dfrac{x}{\cos\theta_{KL}}$.

For the evaluation used here the summation over available volume elements was done in the c.m. system, hence this decay probability factor was written in terms of c.m. quantities (except x). The relevant substitutions for the decay rate were

$$\beta_{KL}\,\gamma_{KL} = \frac{P_{KL}}{M_K}$$

and $P_{KL}\cos\theta_{KL} = \bar{\gamma}\,(P_{KC}\cos\theta_{KC} + \bar{\beta}\,E_{KC})$

to yield the final expression of the probability of decay of K meson in dx at x as

$$\frac{\exp\left\{-\dfrac{x}{\dfrac{c\tau_K}{M_K}\,\bar{\gamma}\,(P_{KC}\cos\theta_{KC}+\beta\,E_{KC})}\right\}dx}{\dfrac{c\tau_K}{M_K}\,\bar{\gamma}\,(P_{KC}\cos\theta_{KC}+\beta\,E_{KC})} .$$

5. For the particles that do decay in the field of view of the telescope there is the question of identification. Here the major counting rate occurred from a particle giving both an upstream and downstream contribution with a mean lifetime near 1.5×10^{-10} sec (early crude estimate). Under the presumption that this represented a θ^0 meson we then had the process $\theta^0 \rightarrow \pi^0 + \pi^0 + 220$ Mev. A certain simplicity exists in the two cascade decays ($\pi^0 \rightarrow \pi^0 + \pi^0$ and $\pi^0 \rightarrow \gamma + \gamma$), leading finally to photons, owing to their isotropic decay patterns. The π^0 decay is of course isotropic in the π^0 system, and in this experiment the θ^0 was taken as isotropic owing to an assumed absence of polarization in the θ^0 frame even if the θ^0 spin were different from zero.

A similar assumption of isotropic decay was used in the trial calculation for other unstable particles. These assumptions then give an isotropic monoenergetic (E^{γ}_0) gamma distribution in the π^0 frame, or an isotropic "rectangular" spectrum of gammas in the K-meson frame, extending from an energy $\gamma_{\pi^0 K} E^{\gamma}_0 (1-\beta_{\pi^0 K})$ to $\gamma_{\pi^0 K} E^{\gamma}_0 (1+\beta_{\pi^0 K})$, or a width $2\beta_{\pi^0 K} \gamma_{\pi^0 K} E^{\gamma}_0$. The $\gamma_{\pi^0 K}$ and $\beta_{\pi^0 K}$ are computed from the Q value of the particular assumed decay mode and $E^{\gamma}_0 \approx 67$ Mev. This spectrum must in turn be transformed into the laboratory system to evaluate the over-all detection efficiency for gammas. For this we recognize that for a given decay mode there are a specific number (N_γ) of resultant gammas per decay event, irrespective of the frame of observation. Hence, a simple change of variables and limits of integration is all that is necessary, providing we retain any dependence on the K meson in terms of c.m. quantities:

$$N_\gamma = \int_{\Omega_{\gamma K}} \int_{E_{\gamma K}} \frac{N_\gamma \, d\Omega_{\gamma K} \, dE_{\gamma K}}{4\pi (2\beta_{\pi^0 K} \gamma_{\pi^0 K} E^{\gamma}_0)}$$

$$= \int_{\Omega_{\gamma L}} \int_{E_{\gamma L}} \frac{N_\gamma \, d\Omega_{\gamma L} \, dE_{\gamma L}}{\gamma_{KL}(1-\beta_{KL}\cos\Theta)\, 4\pi\, (2\beta_{\pi^0 K} \gamma_{\pi^0 K} E^{\gamma}_0)},$$

where the Jacobian $$J = \frac{1}{\gamma_{KL}(1-\beta_{KL}\cos\Theta)}$$

and the new energy limits are

$$E_{\gamma L} \begin{pmatrix} \text{max } + \\ \text{max } - \end{pmatrix} = \frac{\gamma_{\pi^0 K} E^{\gamma}_0 (1 \pm \beta_{\pi^0 K})}{\gamma_{KL}(1-\beta_{KL}\cos\Theta)}$$

In Section 7 it is shown that we have

$$\cos\Theta = \sin\theta_{KL} \cos\phi_{KL}$$

for detection at 90^{o} (lab); hence,

$$\gamma_{KL}(1-\beta_{KL}\cos\Theta) = \frac{1}{M_K}\left\{\bar{\gamma}\,(E_{KC}+\bar{\beta}\,P_{KC}\cos\theta_{KC}) - P_{KC}\sin\theta_{KC}\cos\phi_{KC}\right\}.$$

6. The number of gammas recorded in the laboratory system require that the counter solid angle and counter detection efficiency $\epsilon\ (E_{\gamma L})$ be taken into account in evaluating the integral given in Section 5. In particular the solid angle has the nature of a small increment, so that the integration over solid angle reduces to the product of the integrand and an essentially constant $\Delta\Omega_{\gamma L}$ Therefore we have

$$N_{\gamma)\ \text{observed}} \approx \int \frac{\epsilon\,(E_{\gamma L})\,N_{\gamma}\,dE_{\gamma L}\ \Delta\Omega_{\gamma L}}{4\pi\,\gamma_{KL}(1-\beta_{KL}\cos\Theta)\,2\beta_{\pi^0 K}\,\gamma_{\pi^0 K}\,E_{0\gamma}}$$

7. Now we are in a position to collect the individual terms that enter into the problem. The resulting grand expression for the observed gamma-counting probability for a single K produced then accounts for the probability that the K is emitted into a particular range of θ_{KC}, ϕ_{KC}, E_{KC}; the probability (having the set θ_{KC}, ϕ_{KC}, E_{KC}) that this K meson decays within the field of view of the counter telescope; and, finally, the probability that one of the subsequent gammas reaches the counter and is detected. This expression then must be summed over all the range of θ_{KC}, ϕ_{KC}, E_{KC} available, with of course no contribution from values such that the K cannot pass through the counter field of view (the limits of integration accounted for this). For a particular choice of T_{0L} and of μ (hence N), the expression follows:

$$\frac{dN_\gamma}{dx}\ \text{observed at } x = \int_{E_{KC}} \int_{\theta_{KC}} \int_{\phi_{KC}} \int_{E_{\gamma L}} \left\{ \frac{F(N, E_{KC}) \left(\frac{E^2_{KC}}{M^2_K} - 1 \right)^j}{\left[\int_{E_{KC}} F(N, E_{KC}) \left(\frac{E^2_{KC}}{M^2_K} - 1 \right)^j dE_{KC} \right]} \right.$$

$$\left. \frac{dE_{KC} \cos^k \theta_{KC}\, d\Omega_{KC}}{\left[\iint_{\Omega_{KC}} \cos^k \theta_{KC} d\Omega_{KC} \right]} \right\}$$

$$\cdot \left\{ \frac{\exp \left[- \frac{x}{\frac{c\tau_K}{M_K} \bar{\gamma} (P_{KC} \cos \theta_{KC} + \bar{\beta} E_{KC})} \right]}{\frac{c\tau_K}{M_K} \bar{\gamma} (P_{KC} \cos \theta_{KC} + \bar{\beta} E_{KC})} \right\}$$

$$\cdot \left\{ \frac{\epsilon (E_{\gamma L})\, N_\gamma dE_{\gamma L}\, \Delta\Omega_{\gamma L}}{4\pi (2\beta_{\pi^0 K} \gamma_{\pi^0 K} E^\gamma_0)\, \gamma_{KL} (1 - \beta_{KL} \cos \Theta)} \right\} ,$$

where

$$\Delta\Omega_{\gamma L} = \sin \Theta\, \Delta \Theta\, \Delta \phi,\ \Delta \Theta \equiv \frac{L(\text{Length upper collimator})}{D}\ ,\ \Delta \phi$$

$$\equiv \frac{W\ (\text{width of upper collimation})}{D}\ ,\ \text{and } N_\gamma = 4 \text{ for } \theta^0 \rightarrow \pi^0 + \pi^0 .$$

Also, since $\cos \Theta = \sin \theta_{KL} \cos \phi_{KL}$, we have

$$\sin \Theta = \sqrt{\frac{P^2_{KC} \sin^2 \theta_{KC} \sin^2 \phi_{KC} + \bar{\gamma}^2 (P_{KC} \cos \theta_{KC} + \bar{\beta} E_{KC})^2}{P^2_{KC} \sin^2 \theta_{KC} + \bar{\gamma}^2 (P_{KC} \cos \theta_{KC} + \bar{\beta} E_{KC})^2}} ,$$

and similarly,

$$\gamma_{KL}(1-\beta_{KL}\cos\Theta) = \frac{1}{M_K}\left\{\bar{\gamma}(E_{KC} + \bar{\beta}P_{KC}\cos\theta_{KC}) - P_{KC}\sin\theta_{KC}\cos\phi_{KC}\right\}.$$

Here the small relative variation in D (the distance from K-decay area near the beam axis to the determining collimation near the counter) with K-meson decay position θ_{KC}, ϕ_{KC}, x was neglected. The dimensions were L = 1 in., W = 1.75 in., and $\bar{D}$ = 70 in. The value of Θ was fixed by the value of θ_{KL}, ϕ_{KL} as shown in Fig. 12, since the laboratory direction of the gamma was required to be nearly parallel to the y axis (the counter located at $90^{\circ} \pm 2.5^{\circ}$ (lab), and the transformation involved was from the K-meson frame (traveling along $\theta_{KL}\,\phi_{KL}$) to the lab frame. This required

$$\cos\Theta = \sin\theta_{KL}\cos\phi_{KL}.$$

The choice of order of integration was dictated by functional forms of the limits, and to a certain extent by the fact that a digital computer was used to make the numerical integration. The method used was to evaluate the integrand for each of the mesh of available volume "elements" (θ_{KC}, ϕ_{KC}, E_{KC}) and to sum over the mesh (detail required usually 500 to 1000 elements in a mesh). The integration over the gamma spectrum was done for each volume element (θ_{KC}, ϕ_{KC}, E_{KC}) because of the simple "rectangular" character for an infinitesimal fit. This allowed the machine to look upon the integral

$$\int_{E_{\gamma L}^{min}}^{E_{\gamma L}^{max}} I(\theta_{KC}, \phi_{KC}, E_{KC})\,\epsilon(E_{\gamma L})\,dE_{\gamma L}$$

as equal to $I \int_{E_{\gamma L}^{min}}^{E_{\gamma L}^{max}} \epsilon(E_{\gamma L})\,dE_{\gamma L}$.

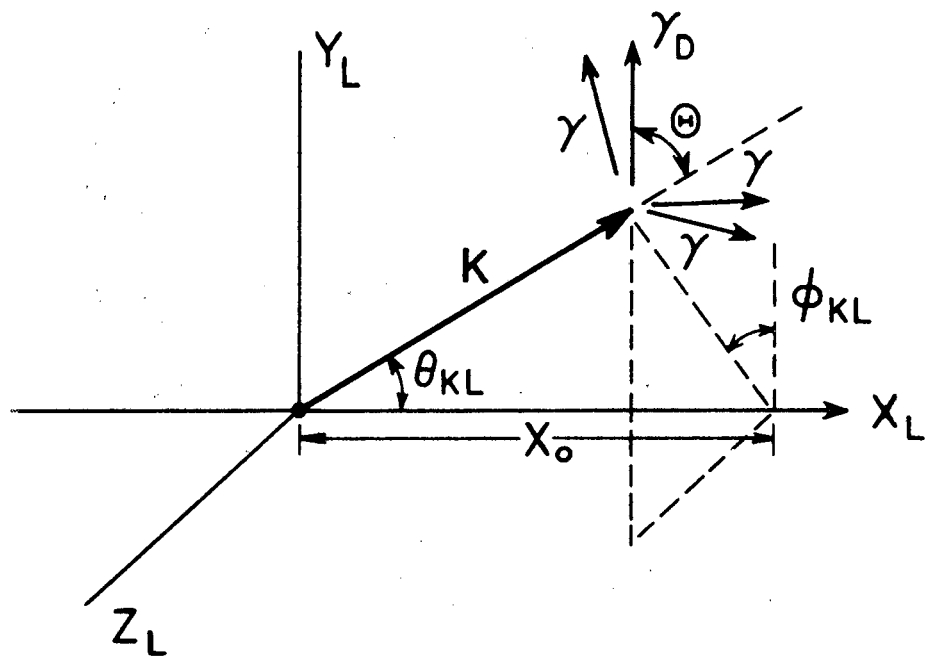

MU-11916

Fig. 12. Decay schematic for strange particle (e.g. $\theta^0 \rightarrow \pi^0 + \pi^0; \pi^0 \rightarrow \gamma + \gamma$), where $\gamma_D \equiv \gamma$ in eligible direction (if counter at X_0), and requires $\cos \Theta = \sin \theta_{KL} \cos \phi_{KL}$.

Further, the value of $E_{\gamma L}^{min}$ fortunately was always below the point $\epsilon\,(E_{\gamma L}) = 0$ (below 40 Mev). Hence, the IBM 650 used the upper limit

$$E_{\gamma L}^{max} = \frac{\gamma_{\pi^0 K} E_0^{\gamma} (1+\beta_{\pi^0 K})}{\gamma_{KL}(1-\beta_{KL}\cos\Theta)}$$

as an address for storage of the integral $\int_0^{E_{\gamma L}^{max}} \epsilon\,(E_\gamma) d\,E_\gamma$ presented in table form, and this reduced the first integration to a simple multiplication for each volume element.

The ϕ integration follows next, with limits dependent on (θ_{KC}, E_{KC}, x, S); namely, the K mesons at θ_{KC}, E_{KC} form a cone in both the c. m. system and the lab system. The rigid collimation, both along the beam and transverse to the beam, allows the telescope to view only particles of this cone decaying within part of the arc, unless the diameter of the cone under consideration is smaller than the transverse collimation determined by the lower defining slit. The ϕ limits involve

$$\phi_{max} = \sin^{-1}\left\{\frac{S\,(2.54)}{2x\tan\theta_{KL}}\right\},$$

or π, depending on the "cone" diameter, are shown schematically in Fig. 13 (where S $\equiv$ lower defining slit width plus fringe, and

$$\tan\theta_{KL} = \frac{P_{KC}\sin\theta_{KC}}{\bar{\gamma}(P_{KC}\sin\theta + \bar{\beta}\,E_{KC})}\Big).$$

Numerically this can be looked upon as

$$2\left\{\int_0^{\phi_{max}} I\,(\theta_{KC},\ \phi_{KC},\ E_{KC})\,d\,\phi_{KC} + \int_{\pi-\phi_{max}}^{\pi} I\,(\theta_{KC},\ \phi_{KC},\ E_{KC})\,d\,\phi_{KC}\right\}.$$

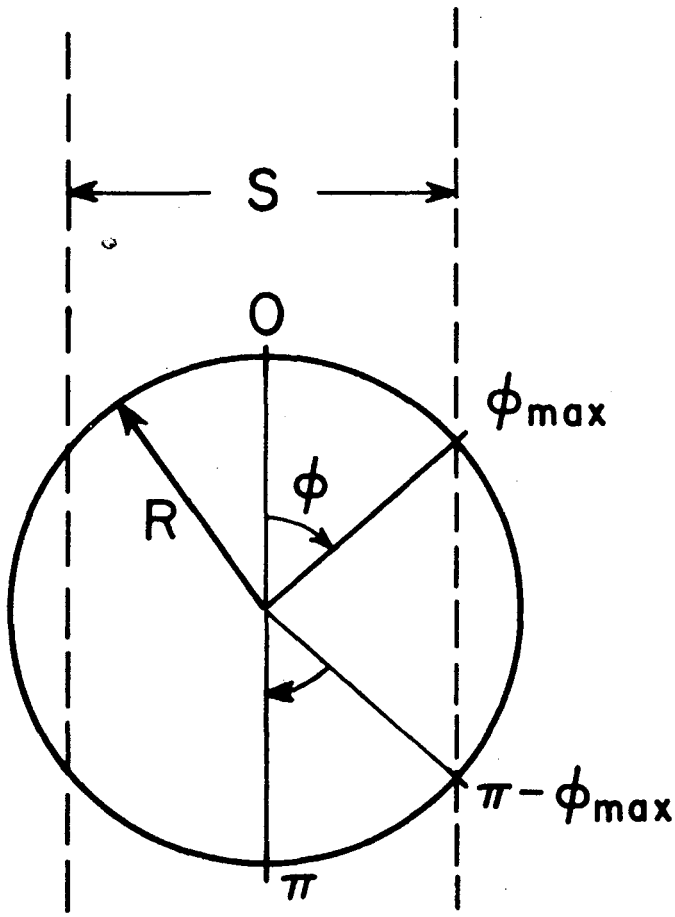

MU-11917

Fig. 13. Limits on ϕ integration, where
$S \equiv$ lower defining collimation width plus fringe correction,
$R = X_L \tan \theta_{KL}$
and
$$\phi_{max} = \sin^{-1} \frac{S}{2X_L \tan \theta_{KL}}$$

The θ_{KC} integration proceeds next, with limits dependent only on E_{KC} and x. For positive values of x the limits are from 0 to θ_{max}, with $\theta_{max} = \pi$ or $\cos^{-1}(-\bar{\beta}/\beta_{KC})$, depending on whether we have $\beta_{KC} \leq \bar{\beta}$ or $\beta_{KC} > \bar{\beta}$. For negative values of x the limits include only those K particles (impossible for hyperons) coming out in the backward hemisphere in the laboratory system; namely, from $\cos^{-1}(-\bar{\beta}/\beta_{KC})$ to π (no contribution, of course with $\beta_{KC} < \bar{\beta}$).

Finally the limits on E_{KC} are determined by the total energy N available in the c.m. system and the specific reaction in question. In the c.m. system these limits are very simple, and may be written for the reaction $P + n \rightarrow n + Y + K$ as M_K to

$$E_{KC}^{max} = \frac{N^2 - (M_n + M_Y)^2 + M_K^2}{2N} .$$

The "integrations" over T_{0L} and N (or μ) were accomplished by numerical methods, with values interpolated on the basis of smooth calculated curves for specific choices N and T_{0L}. This was simplified somewhat through the use of a composite N distribution that took into account both the distribution in T_{0L} and the Fermi internal-momentun distribution, when it was found that the effect of a small variation in T_{0L} with N constant was only a rather small correction factor. In addition, a numerical integration over x. was done to account for both the target thickness and the collimation bite.

The calculation outlined above allows one to predict the expected counting rate of the counter telescope for a specific position. This gives the detection efficiency per produced θ^0 decaying by the mode $\theta^0 \rightarrow \pi^0 + \pi^0$. Similar analysis holds for other competing strange particles. This information, the known target thickness, and the incident proton beam fix the cross section directly. A more elegant way of putting the cross section is as follows (averaged over a range of T_{0L}):

$$\overline{\frac{d^2\sigma}{dE_{KC}d\Omega_{KC}}} = \frac{2\pi}{\hbar} \int_{\mu_{min}}^{\mu_{max}} \int_{T_{0L}}^{T_{0L}^{max}} \frac{|H|^2}{V\,(\text{relative velocity})}$$

$$f(\mu)\, g(T_{0L})\, F(N, E_{KC})\, d\mu\, d\, T_{0L}.$$

This allows one to observe the T_{0L} and μ (or N) averaging processes done by numerical integration in the analysis above. The approach here was of course not through a known $/H/^2$ but by comparison to experimental data with various trial expressions used for $/H/^2$.

BIBLIOGRAPHY

1. G. D. Rochester and C. C. Butler, Nature 160, 855 (1947).
2. Conferenza Internazionale Solle Particelle Elementari, il Nuovo Cimento, Pisa 1955.
3. Alvarez, Crawford, Good, and Stevenson, Phys. Rev. 101, 503 (1956).
4. W. B. Fowler, Private Communication, University of California Radiation Laboratory, April 1956.
5. S. Goldhaber in Proceedings of the Sixth Annual Rochester Conference; Preprint, 1956.
6. M. Gell-Mann, Phys. Rev. 92, 833 (1953); "The Interpretation of New Particles as Displaced Charge Multiplets," Institute for Advanced Study, Princeton, 1955.
7. M. Gell-Mann and A. Pais, Proceedings of 1954 Glasgow Conference on Nuclear and Meson Physics (p. 342). Pergamon Press, London, 1955.
8. R. G. Sachs, Phys. Rev. 99, 1576 (1955)
9. M. Goldhaber, Phys Rev. 92, 1279 (1953); Phys. Rev. 101, 433 (1956)
10. R. K. Squire, "Characteristics of the Production of Neutral Pions Near Threshold in p-p Collisions" (Thesis), UCRL-3137, Sept. 1955.
11. Annual Reviews of Nuclear Science, Vol. 4 (p. 111), Annual Reviews Inc., Stanford (1954).
12. Progress in Nuclear Physics, Vol. 3 (p. 84), Academic Press Inc., New York, 1953.
13. "Multiple Coincidence and Anticoincidence Circuit", Counting Note UCRL File No. CC 3-1, 1956.
14. Friedlander, Hudis, and Wolfgang, Phys. Rev. 99, 263 (1955)
15. W. Heitler, "The Quantum Theory of Radiation," Third Edition, Oxford Press, London 1953.
16. Gupta, Snyder, and Chang, Bull. Am. Phys. Soc. II, 1, No. 4. 186 (1956).

17. G. Wenzel, Phys. Rev. 101, 1215 (1956).
18. G. Takeder, Phys. Rev. 101, 1547 (1956).
19. Leitner, Chrétien, Samios, Schwartz, and Steinberger, Bull, Am. Phys. Soc. II, 1, No. 4, 186 (1956).
20. S. L. Collins and G. B. Ridgeway, Page 389 of "Mesons and Fields", Bethe and de Hoffman, Row, Peterson and Co., Evanston, Illinois, June 1955.
21. Block, Harth, and Sternheimer, Phys. Rev. 100, 324 (1955).
22. J. Blaton, Dansk.-Vid. Selsk. 24 No. 20 (1950).
23. E. Fermi, "Elementary Particles," Yale University Press, New Haven, 1951.
24. J. V. Lepore, and M. Neuman, A Statistical Model for High-Energy Events, UCRL-2649, July 1954.